Thesis

Master in Chemical Engineering

CFD modelling of Gas-Liquid Cylindrical Cyclones (GLCC),

Geometry analysis

Juan Carlos Berrío Betancourt

Advisor:
Nicolás Ratkovich, Ph.D.
Universidad de los Andes

Universidad de los Andes

November 2016

Abstract

The Gas-Liquid Cylindrical Cyclone (GLCC) is one of the main alternative of conventional vessel-type separators of a two-phase gas-liquid mixture, since it has attractive characteristics, as it is more compact, simple and has a lower footprint. The main limitation for this separator is that is not fully studied. The main objective of this study is to use CFD modelling, in STAR-CCM+ software, in order to evaluate the effect of geometrical modifications in the reduction of LCO and GCU.

CFD simulations for single-phase flow are carried out in order to validate the swirling flow from experimental data acquired by *Erdal (2001).* Axial and tangential velocities profiles are compared, obtaining fair agreement. CFD simulations for two-phase flow were done under zero net liquid flow. The average liquid holdup is compared with *Kanshio (2015)* experimental data, under different inlet superficial gas velocities. A good agreement is obtained between experimental data and CFD simulations, with RMS errors around 13%. From this CFD model it is found that using a sharpening factor with a value of 1, describes better the experimental data due to the reduction of numerical diffusion.

An experimental setup is built in order to validate a CFD model that includes both faces entering to the GLCC. LCO data is acquired and pressure transmitters are used at each outlet to define properly the boundary conditions. An error below 6% is obtained comparing CFD simulations with experimental data. Once the model is validated, five geometrical variables are defined, and tested with CFD. Those variables are the inclination angle of the tangential inlet, the height of the tangential inlet, the effect of including a dual inlet, the influence of including a nozzle or reduction in area at the inlet and the effect of including a volute inlet with rectangular slot. It is found that the best options of the evaluated levels are an angle of 27°, the inlet located 10 cm above the center, a dual inlet with 20 cm of spacing between both inlets, a nozzle of 3.5 cm of diameter and a volute inlet of 15% of pipe area. The combination of these options in the same geometry reduced LCO in 98%. Finally, the swirling decaying is studied with vector velocities profiles along the GLCC and is found that liquid seems to has a greater impact than gas. Values of Reynolds number around 250 seems to avoid swirl generation.

TABLE OF CONTENT

1. Introduction

One of the main issues in the oil and gas industry is the separation of the multiphase flow coming from oil wells. In a typical reservoir, it can be found oil, gas and water. The quantities of each phase varies with time, reducing the oil and gas fraction and increasing the water fraction (known as water cut). In mature oil wells, the water cut can reach values up to 90% (Frising *et al*., 2005). This work focuses on the study of the separation of a two-phase gas-liquid mixture. The liquid can be oil, water or a mixture of them. The separation of this mixture is critical for transportation and further processing. The gas is treated to be re-injected or used as a fuel. Oil is stabilized before is transported to refineries. Finally, the water is treated to be disposed or re-injected to maintain the reservoir pressure. Due to environmental regulations and laws, re-injected water has to reach certain specifications.

Traditionally, the separation was performed on a vessel-type separator, which have good separation efficiencies, but are heavy, bulky (large footprint), expensive, and have high hydraulic retention time. This is a real problem for off-shores installations due to the fact that they have limited footprint. With the increasing number offshore facilities, the design of a compact separator has been highly studied (Hreiz *et al*., 2011). One of the main alternatives to conventional vessel-type separators is the Gas-Liquid Cylindrical Cyclone (GLCC) developed by Tulsa University (OK, USA) and Chevron. This separator consists on a cylindrical vertical pipe with a middle height tangential inclined inlet and two outlets. One outlet is located at the top for the gas phase, and the other one is at the bottom for the liquid phase. Due to the tangential inlet, the flow inside the cyclone creates a swirl that helps to separate the gas and liquid. Compared to vessel type separators the GLCC is much more compact, simple, has a lower weight, cost and footprint (Shoham *et al*., 1998). Despite these advantages, the GLCC is not widely used in oil and gas industry owing to the lack of a predictive performance model that allows a proper design. Additionally, many of the phenomena inside the cyclone are not fully understood (Hreiz *et al*., 2014). Gas/Liquid separation performance is generally is characterized by two parameters, namely, liquid carry-over (LCO) and gas carry-under (GCU). The first one is the amount of liquid that leaves the separator in the upper outlet with the gas as main phase. The second one is the amount of gas that leaves the separator in the lower outlet with the liquid as main phase. Both phenomena limited proper operation of the GLCC (Gomez, 2001). Other main factor to consider in the design and study of a GLCC is the Reynolds number. At high viscosities or low velocities, or both of them, the Reynolds number decreases and the flow could pass

from a turbulent to a laminar regime. Velocity profiles inside the separator are affected and the swirl flow decays faster as Reynolds number decreases. This represents a big problem since the velocity profile could turn into a pipe flow (no rotation) and the separation principle of a GLCC is lost (Gomez, 2001).

Computational Fluid Dynamics (CFD) can be a useful tool to study the hydrodynamics of two-phase flow and the phenomena of GCU and LCO. As it can be seen in state of the art, CFD modelling of the GLCC can be possible and it obtains reliable results. As in all CFD modelling studies, the validation of the model with experimental data is essential to produce an appropriate analysis. One of main advantages of CFD modelling is feasibility to study different operational conditions, geometry, two-phase flow inlet characteristics and other issues, without the complications that these changes may represent to an experimental setup. This research project seek to study the effect of different characteristics and parameters related to the GLCC working conditions in the LCO and GCU using CFD modelling.

2. Objectives

This section presents the general and specific objectives as follows:

2.1. General objective

To study the effect of different operating and geometrical conditions in the liquid carry-over and gas carry-under in a GLCC using CFD modelling.

2.2. Specifics objectives

- To generate a CFD model capable to reproduce experimental data (tangential and axial velocities) under different operating conditions.
- To study the effect of low Reynolds number and its relationship with the decaying of swirl flow into pipe flow.
- To evaluate geometrical conditions that reduces liquid carry-over and gas carry-under in a GLCC, such as single vs dual inlet effect and an inclined volute inlet with rectangular slot.

3. State of the art

This section presents the most relevant studies on the GLCC.

3.1. Gas-Liquid Cylindrical Cyclone (GLCC)

The GLCC is a cylindrical vertical pipe separator with a downward inclined tangential inlet located near to the middle height of the pipe. It has two outlets located at the top and the bottom, for gas and liquid phases, respectively. Figure 1 shows a schematic representation of typical GLCC. The geometry and the location of the tangential inlet create a swirl that generate centrifugal forces over the fluids. In conjunction with gravitational forces, the liquid is carried toward the wall of the pipe and pushed down to the bottom outlet. For the upper part, the gas trend to flow in the center while the liquid droplets impact at the wall draining towards the liquid (Movafaghian, 1997).

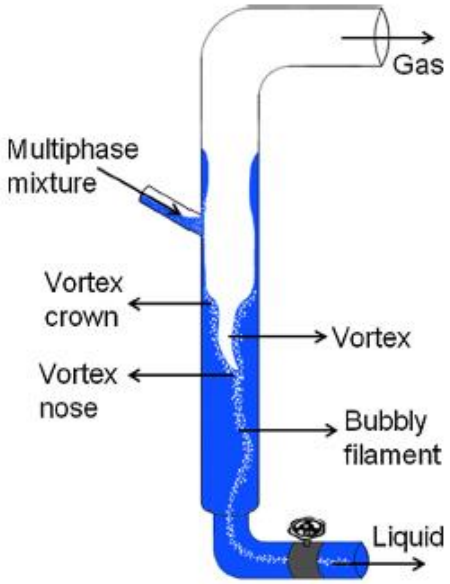

Figure 1. GLCC schematic representation (Hreiz et al, 2014)

As it does not has any moving part or any complex internal device, the cost of the equipment is low in comparison against a conventional vessel-type separator. Additionally the GLCC is a compact separator for the reason that it has shorter fluid retention time, this is the reason it has a lower weight and occupies less volume than traditional separators. In limited space operations as in offshore installations, this compact separator seems to provide a great solution to space problem. Figure 2 shows a size comparison between the GLCC and conventional horizontal and vertical vessel-type separators.

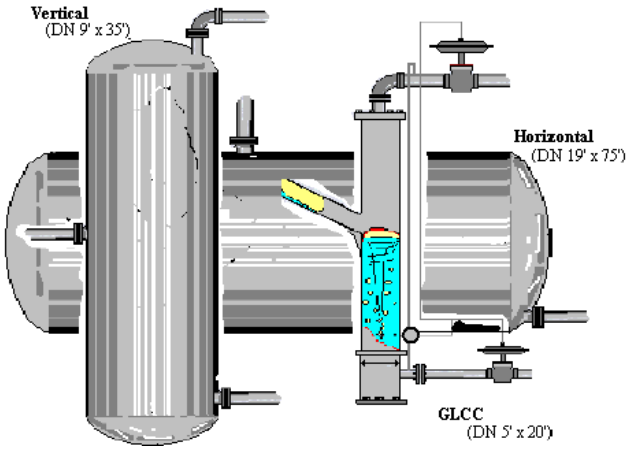

Figure 2. Size comparison between GLCC and conventional vessel-type separators (CADETEP, Universidad Simón Bolívar)

3.2. GLCC applications

The GLCC has many applications in the petrochemical industry. It can be used as a full separator of the multiphase flow or as partial separator as a previous stage of a different process. Used as a partial separator it enhances the performance of multiphase pumps and desanders (Mantilla, 1998).One common GLCC application is for multiphase metering. The flow, which is desired to be measured, passes through the separator and single-phase flow meter are used at each outlet. Then the flow is recombined just after to continue in the pipeline. This is an important application owing to the cost and complexity of multiphase meters (Movafaghian *et al*., 2000). Other applications are automatic well-testing, slug flow dissipation and wet gas applications. This compact separator could be suitable not only for offshore operations, but it can be useful in onshore operations as well. Additionally, the GLCC has many other applications in gas-liquid mixtures not related with oil and gas industry. The same operational and theoretical principle is used in separators of other multiphase mixtures such as foam flow (Guzmán, 2005).

3.3. Liquid Carry-Over (LCO) and Gas Carry-Under (GCU)

Two major problems that affect directly the separation efficiency of a GLCC are the LCO and the GCU. LCO is the phenomena of liquid droplet presence in the stream of gas at the top of the separator. Typically, this situation occurs when the GLCC is operating under extreme condition of high gas or liquid flow rates. In addition, it is extremely dependent on the flow pattern in the upper part of the separator. An operational envelope of LCO can be obtained by plotting liquid flow rate against the gas flow rate at which the phenomena starts. The region below the curve represents good operational conditions and good separation

efficiencies, as there is not LCO phenomena. Above the curve represents the region of continuous LCO (Adebare, 2006). Figure 3 shows an example of a LCO operational envelope, where Q_L is the flowrate of liquid, V_{sL} is the superficial liquid velocity, Q_G is the flowrate of gas and V_{sG} is the superficial gas velocity.

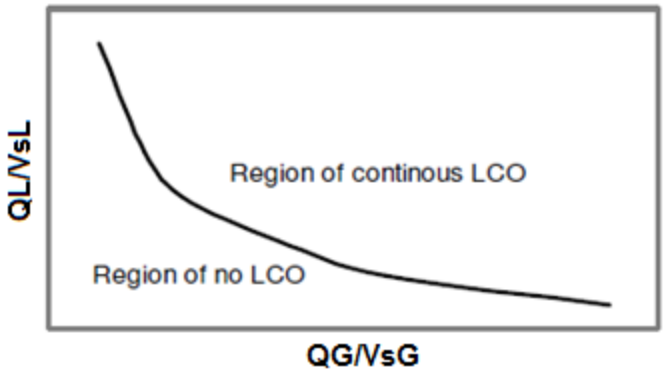

Figure 3. LCO operational envelope (Adebare, 2006)

On the other hand, the GCU is the phenomena of gas bubbles presence at the liquid stream at the bottom of the separator. A gas-core filament is formed due to the movement of bubbles at the lower part of the GLCC as a consequence of the swirl. The tangential inlet and the fluid velocity has a direct impact on the gas-core formation. There are three mechanisms that have been identified to have possible responsibility on the GCU: (i) Shallow bubble trajectories prevent small bubbles from escaping to the gas-core filament. (ii) Due to the instability of rotational flow, there is a breaking of the gas-core filament near to liquid exit, and (iii) High flows of liquid can produce a concentrated cloud of bubbles that do not move to the gas core and are carried with the liquid to the exit (Shoham *et al*., 1998).

3.4. Zero-net liquid flow

Before LCO occurs in a GLCC, zero-net liquid flow takes place in the upper part of the separator. This phenomenon is the production of only gas in the upper outlet, but with liquid remaining between above the inlet and the gas outlet. The liquid volume fraction in this zone is called zero net liquid holdup (Arpandi, 1995). When this condition is reached in a GLLC the liquid that flow upwards can change its direction before leaving the separator. For this reason, zero-net liquid flow is an important parameter since it is the limit before LCO occurs. Additionally, this concept is relevant in order to estimate, mixture density and pressure drop predictions in several mechanistic models (Kanshio *et al.*, 2015)

3.5. Reynolds number effect

The Reynolds number is an important issue to be considered in a GLCC for the reason that it has a direct effect on the separation efficiency. When the inlet fluid has a low Reynolds number (as consequence of high viscosity liquid or low flow velocity) the swirling decay quickly and only free gas is separated. The axial and tangential velocity profiles get modified as the swirling decay occurs faster. With no rotation, there are null centrifugal forces that are essential to reach the phase separation (Gomez, 2001).

3.6. Literature review – previous studies

The GLCC has been specially studied by the University of Tulsa. *Arpandi (1995)* developed a mechanistic model for the prediction of main features of the hydrodynamics of a GLCC. He built an experimental setup in order to acquired data such us equilibrium level, zero-net liquid flow holdup and operational envelope to validate the mechanistic model. *Marti et al. (1996)* studied the GCU and developed a mechanistic model to predict this phenomenon and the interface of the two phases. Moreover, they studied the bubble trajectory and performed a preliminary CFD simulation using CFX software. *Movafaghian (1997 and 2000)* developed an experimental setup to study the effects of geometry, fluid properties and pressure on the flow hydrodynamics. Additionally the data obtained were used to refine a mechanistic model done previously. *Shoham et al. (1998)* summarizes experimental and computational studies done. They found that the inlet design plays an important role for the reason that it determines the distribution of both phases. Related to LCO, they found that is dependent on the flow pattern in the upper part. About the GCU, they found three mechanisms that contributed to the phenomena, but they are not studied at all. *Mantilla (1998)* developed correlations to predict swirl intensity decay and tangential and axial velocities distributions. He focused on the improvement of previously developed bubble trajectory models. *Steenbergen et al. (1998)* studied the rate of decay of swirl in turbulent pipe flow due to an experimental setup. They used two different Reynolds numbers and two inlet conditions. As conclusion, they found that Reynolds number affects the rate of decay. *Erdal (1997)* performed CFD simulations of single and two-phase flow in GLCC. The results were compared with experimental data showing good agreement. *Erdal et al. (1998)* developed CFD simulations to study the free interface region in the GLCC, the results were compared with flow visualization experiments. *Erdal et al. (2000)* studied the behavior of small bubbles in the lower part of the GLCC by CFD simulations. They studied the effect on certain parameters as Reynolds number, and some velocities. *Chirinos et al. (2000)*

developed a mechanistic model to predict the percent of LCO under a special flow conditions. Furthermore, they extend a previous model to predict operational envelope for LCO under high pressure conditions. They compare the results with experimental data and obtained good agreement. *Erdal (2001)* developed a complete experimental and computational study. With an experimental setup turbulent kinetic energy, tangential and axial velocities were measured in different points of the GLCC and under different flow conditions. Moreover, CFD simulations were developed to perform similar analysis as in previous works. *Gomez (2001)* developed a mechanistic model to predict the GCU in a dispersed two-phase swirling flow. He performed experiments to validate the model. *Avila et al. (2003)* performed a mathematical model and control study of a three-phase separation system. The first part of the studied system was a GLCC with the liquid exit connected to another compact separator to split water from oil. *Guzman (2005)* developed a different study related with foam flow. This flow is formed by gas bubbles dispersed in a continuous liquid phase. A mechanistic model to predict aqueous foam formation was done and validated with experimental data. *Najafi et al. (2005)* developed a comparison between turbulence models in order to predict the swirling decay under different operating conditions. They validated the results with an experimental setup. *Adebare (2006)* studied the effects of fluid properties such as density, foam, and emulsion formation over separation targets as zero net gas flow, zero net liquid flow and LCO. The study was accomplished by an experimental setup with foamy oil as multiphase flow. *Gupta et al. (2006)* performed CFD simulations varying the Reynolds number and the inlet aspect ratio in a cylinder. They compared the results with experimental data and found that Reynolds number do not have great effect on swirling flow. *Brito et al. (2009)* developed a bibliographical research to analyze the effect of viscosity in separators. They found that the separation efficiency is diminished with higher viscosities. *Hreiz et al. (2011)* developed a CFD model to study the swirling flow. The results were validated with experimental data of Erdal experiments. Later, *Hreiz et al. (2013)* built an experimental setup to study the effect of the nozzle design at the inlet. They realized that the nozzle is a key parameter that affects the GLCC hydrodynamics and the phase's separation due to GCU and LCO phenomena. Afterwards, *Hreiz et al. (2014)* developed an experimental analysis of the flow hydrodynamics. They found very complex results as the vortex vary from laminar to turbulent regime and vice versa. As conclusion they propose multiple tangential inlets to improve separation efficiency. *Kanshio et al. (2015)* built an experimental setup to study the liquid holdup with an electrical resistance tomography and a wire mesh sensor. They found that the inlet gas velocity and

liquid holdup had a great influence in the flow behavior in the upper section of the separator. Table 1 and Table 2 summarize the previous works reported before.

Table 1. Summary of previous works done on GLCC

Author	Study type	Objective	Fluids	Turbulence model
Arpandi (1995)	Mechanistic model and experimental study	Develop predictive models for hydrodynamics of multiphase flow.	Water and air	-
Marti et al. (1996)	Mechanistic model and CFD	Study GCU, interface and bubble trajectory.	Water	N/A
Steenbergen et al. (1998)	Experimental study	Study the rate of decay of swirl in turbulent flow.	Water	-
Movafaghian (1997 and 2000)	Experimental and mechanistic model	Study the effects of geometry, fluid properties and pressure.	Water and air	-
Erdal (1997)	CFD simulations with experimental validation	Study single phase and two phase flow.	Water and air	k-ε model
Shoham et al. (1998)	State of the art of experimental and computational studies	Summarizes main issues of experimental and computational studies done.	-	-
Mantilla (1998)	Theoretical, mathematical model and CFD	Correlations for swirl intensity decay, axial and tangential velocities.	N/A	k-ε model
Erdal et al. (1998)	CFD simulations with experimental validation	Study free interface region.	Water and air	k-ε model
Erdal et al. (2000)	CFD simulations	Study the behavior of small bubbles in the lower regions.	Water and air	k-ε model
Chirinos et al. (2000)	Mechanistic model and experimental validation	Study LCO.	Water and air	-
Erdal (2001)	Experimental setup and CFD simulations	Study of inlet configuration, inlet flow and viscosity for single-phase flow.	Water/Glycerin and air	k-ε model

Table 2. Continuation of summary of previous works done on GLCC

Author	Study type	Objective	Fluids	Turbulence model
Gomez (2001)	Mechanistic model and experimental validation	Study the hydrodynamics of dispersed two-phase swirling flow in the lower part of the GLCC.	Water/oil and air	-
Avila et al. (2003)	Mathematical model and control	Study control of a three-phase separator, the first part is a GLCC.	Water, oil and air	-
Guzman (2005)	Mechanistic model and experimental validation	Study foam flow.	Water, air and surfactant	-
Najafi et al. (2005)	CFD simulations and experimental setup	Study turbulence models in order to predict swirling decay.	Water	k-ε, Reynolds stress models
Adebare (2006)	Experimental setup	Study the effect of fluid properties to optimize the GLCC.	Water/oil and air	
Gupta et al. (2006)	CFD simulations and experimental setup	Study the flow in a cylinder under different Reynolds numbers and inlet aspect ratios.	Water	k-ε model
Brito (2009)	State of the art	Study the effect of viscosity.	-	-
Hreiz et al. (2011)	CFD simulations with experimental validation	Study swirling flow.	Water and glycerin	Spalart-Allmaras, k-ε, k-ω and Reynolds stress models
Hreiz et al. (2013)	Experimental setup	Study the effect of the inlet nozzle design.	Water, air and surfactant	-
Hreiz et al. (2014)	Experimental setup	Study flow hydrodynamics.	Water and air	-
Kanshio et al. (2015)	Experimental setup	Study of liquid holdup under different flow conditions.	Water and air	-

3.7. Computational Fluid Dynamics (CFD)

Modelling different processes and units of a process in CFD is an important tool in order to study the fluid flow, heat transfer and other phenomena such as a chemical reaction. In this case, the study of a GLCC in CFD can be done as it is demonstrated in the literature review. CFD is used as an extra resource in order to analyze and understand flow behavior and other important issues inside the equipment. Additionally, it can be used as a design test to

prove changes in geometry, operating conditions, fluid properties and any other variation that would like to be tested. In all CFD simulations is essential to validate the model with experimental data or previous works done to assure reliable results. In order to perform a CFD simulation, three stages have to be done: (i) pre-processing, (ii) solver (iii) post-processing (Versteeg *et al*., 2007).

3.7.1. Pre-processing

This stage consists in the input parameters and specifications of the problem. The first step is the definition of the geometry of the region of interest. This can be done in the same CFD software or in a special Computer-Aided Design (CAD) software, such as Autodesk Inventor® 2015. The second step is the grid or mesh generation. This is an essential issue of a CFD simulation for the reason that proper results depend on a good mesh. A mesh is the subdivision of the geometric domain in cells or control volumes were each of the equations that represents the phenomena of study is solved. A poor mesh (small number of elements) can obtain a quick solution, but not well at all, while an extra-fine mesh (large number of elements) can obtain very good results, but in a large period of time. For this reason, a grid independence test should be performed in order to define an adequate mesh size. The test consists on running simulations varying the mesh size and comparing the obtained results. The selected mesh size is the one with the less computational time and no evidence of a significant variation in the results. The third step is the selection of the physical and chemical phenomena that need to be modelled. The fourth step is the definition of fluid properties and the last step is the specification and definition of the boundary conditions (Versteeg *et al*., 2007).

3.7.2. Solver

There exist many kind of numerical solution techniques, but in most of the CFD software is used the finite volume method. This method refers that each cell of the mesh represents a volume control used to integrate the differential equations that describes flows behavior. The numerical algorithm consists of three steps: (i) Integration of the governing equations of fluid flow over the control volumes. (ii) Discretization of the resulting equations of step one into a system of algebraic equation. This process can be done by many discretization techniques and schemes. (iii) Solution of the resulting equations of step two by an iterative method as the equations are complex and strongly non-linear. Due to the solution is found by an iterative method, it is important to define a tolerance to the desired difference between the

results from one iteration to another. This difference is evaluated for velocities, continuity, energy and other important terms and are called the residuals (Versteeg *et al*., 2007).

3.7.3. Post-processing

This stage consists in the acquisition from the simulation the desired information that is wanted to be analyzed. With the development of CFD commercial software, more visualization data tools are available for post-processing. The most common visualized information are domain of geometry, grid display, vector plots, contour plots, 2D or 3D surface plots and particles tracking. The animations and videos showing the evolution of a property in time are as well considered in this stage (Versteeg *et al*., 2007).

3.8. Governing equations

The equations that described the motion of the fluid are known as Navier-Stokes equations, which represents a momentum balance. Equations (1) to (3) show the momentum balance for each dimension for a compressible Newtonian fluid.

$$x\ axis\text{:}\ \frac{\partial(\rho u)}{\partial t} + div(\rho u \mathrm{u}) = -\frac{\partial p}{\partial x} + div(\mu\ grad\ u) + S_{Mx} \tag{1}$$

$$y\ axis\text{:}\ \frac{\partial(\rho v)}{\partial t} + div(\rho v \mathrm{u}) = -\frac{\partial p}{\partial y} + div(\mu\ grad\ v) + S_{My} \tag{2}$$

$$z\ axis\text{:}\ \frac{\partial(\rho w)}{\partial t} + div(\rho w \mathrm{u}) = -\frac{\partial p}{\partial z} + div(\mu\ grad\ w) + S_{Mz} \tag{3}$$

Where u, v, w are the components of velocity in each axis, ρ is the fluid density, p is the pressure, μ is the fluid dynamic viscosity and S_M is a momentum source term for each axis. The mass conservativeness principle is assured by the continuity equation shown in equation (4) for a compressible Newtonian fluid.

$$\frac{\partial \rho}{dt} + div(\rho \mathrm{u}) = 0 \tag{4}$$

If an assumption of incompressible fluid is realized, the density will remain constant along time.

If the Reynolds number is big enough, the flow is in turbulent regime and the previous shown equations have to be modified. As in a GLCC the flow regime in most cases is turbulent, this subject need to be considered. To consider this modifications, the Reynolds-averaged Navier-Stokes equations (RANS) are used. Those equations are shown in equations (5) to (7).

$$\frac{\partial(\bar{\rho}U)}{\partial t} + div(\bar{\rho}U\mathrm{U}) = -\frac{\partial \bar{p}}{\partial x} + div(\mu\ grad\ U) + \left[-\frac{\partial\overline{(\bar{\rho}u'^2)}}{\partial x} - \frac{\partial\overline{(\bar{\rho}u'v')}}{\partial y} - \frac{\partial\overline{(\bar{\rho}u'w')}}{\partial z}\right] \quad (5)$$

$$\frac{\partial(\bar{\rho}V)}{\partial t} + div(\bar{\rho}V\mathrm{U}) = -\frac{\partial \bar{p}}{\partial y} + div(\mu\ grad\ V) + \left[-\frac{\partial\overline{(\bar{\rho}u'v')}}{\partial x} - \frac{\partial\overline{(\bar{\rho}v'^2)}}{\partial y} - \frac{\partial\overline{(\bar{\rho}u'w')}}{\partial z}\right] \quad (6)$$

$$\frac{\partial(\bar{\rho}W)}{\partial t} + div(\bar{\rho}W\mathrm{U}) = -\frac{\partial \bar{p}}{\partial z} + div(\mu\ grad\ W) + \left[-\frac{\partial\overline{(\bar{\rho}u'w')}}{\partial x} - \frac{\partial\overline{(\bar{\rho}v'w')}}{\partial y} - \frac{\partial\overline{(\bar{\rho}w'^2)}}{\partial z}\right] \quad (7)$$

The over bar indicates that the variables are time-averaged and the tilde represents averaged properties. The additional terms, comparing Navier-Stokes equations and RANS are known as Reynolds stresses. To calculate this stresses multiple turbulence models exist and are classified due to the number of extra equations added. Table 3 summarizes some turbulence models.

Table 3. Reynolds turbulence models (Versteeg et al., 2007)

Number of extra transport equations	Name
Zero	Mixing length model
One	Spalart-Allmaras model
Two	k-ε model k-ω model Algebraic stress model
Seven	Reynolds stress model

4. Methodology

In this section, the main features about the configuration used for the CFD simulations are described. The software used is STAR-CCM+ v11.02. Two main cases are evaluated; a single-phase flow model and a two-phase flow model. For the two-phase flow model, one literature case is used, and an experimental setup is built in order to validate the CFD model. After the validation is done, modifications in the geometry of the GLCC are evaluated using the same CFD model.

4.1. Single-phase flow

For the single-phase flow case, the experimental setup done by *Erdal (2001)* is used. This GLCC only includes the bottom of the separator.

4.1.1. Experimental data acquisition setup performed by *Erdal (2001)*

Turbulent kinetic energy, tangential and axial velocities were parameters measured in the experimental setup by a Laser Doppler Velocimeter (LDV). Twenty-four measurement points were acquired, those points were located on a measurement plane between 0.32 m and 0.9 m below the inlet. The effect of four different parameters over hydrodynamics were analyzed by *Erdal (2001)*. Those parameters were inlet configuration, inlet-outlet orientation, inlet flow rate and viscosity. Three-inlet configuration were considered, namely, a single inclined inlet, two inclined inlet and one gradually reduced inlet nozzle. Two inlet-outlet orientation were studied; one is rotated 180° along the axis from the other. Three flow rates were evaluated, 0.000631, 0.00189 and 0.00454 m^3/s and two viscosities, 1cP (water) and 7cP. The fluid used to reach the second viscosity value was a mixture of water and glycerin. It is important to say that the experiments were carried with a single-phase flow of water (Erdal, 2001). Figure 4 shows the schematic representation of the geometry used by *Erdal (2001).*

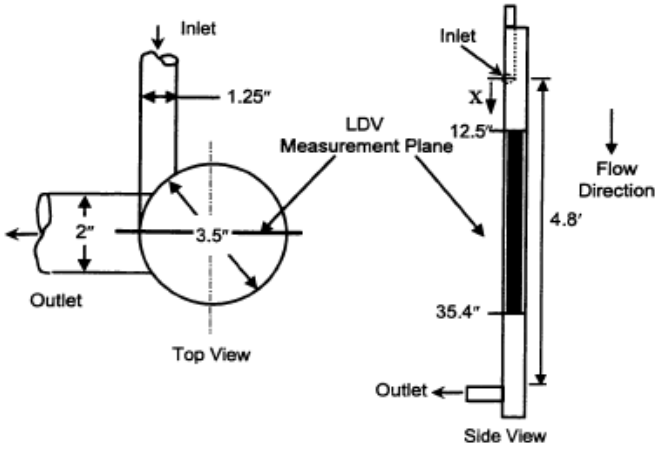

Figure 4. Experimental apparatus of Erdal (2001)

4.1.2. Geometry

For the geometry of *Erdal (2001)* only half of the separator is considered (lower part) to replicate the dimensions used experimentally. The GLCC body has a radius of 0.0445 m and a total height of 1.715 m. The radius of the tangential inlet and the outlet measure 0.016 m and 0.038 m respectively. Figure 5 shows from different views the geometry done.

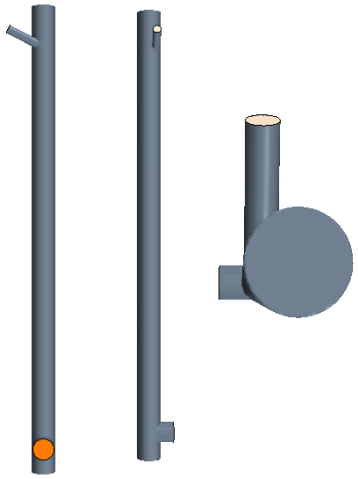

Figure 5. Lateral view, frontal view and top view of the geometry for the case of Erdal (2001)

4.1.3. Mesh

Hreiz et al. (2011) found that a combination of a tetrahedral and hexahedral grid was adequate for this kind of problem. Based on this, a polyhedral grid is selected in STAR-CCM+. This grid provides a balanced solution for complex problems and gets approximately five times fewer cells than a tetrahedral mesh (CD-Adapco, 2016). In order to improve the accuracy of the solution near to the wall, the prism layer mesher model is selected. This model generates orthogonal cells in wall surfaces. As it was mentioned on previous section, a grid independence test is needed in order to select an adequate mesh size. For this reason and based in the work done by *Celik et al. (2008)*, three different mesh are proved. A coarse mesh with 152,047 cells, a normal mesh with 495,440 cells and a fine mesh with 891,838 cells. The grids used for the independence test are shown in Figure 6.

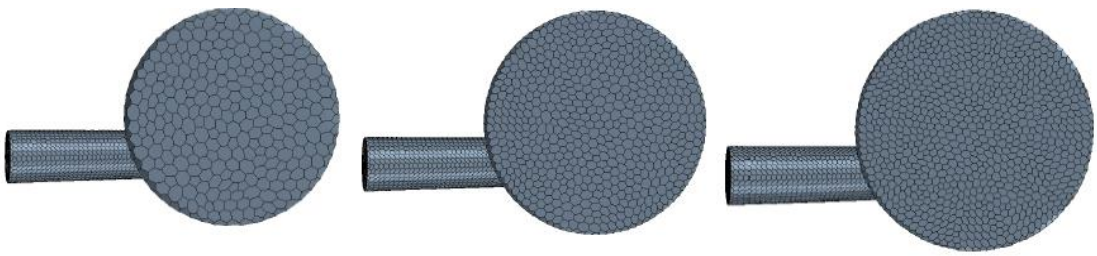

(a) (b) (c)

Figure 6. Meshes used for the grid independence test: (a) Coarse mesh, (b) Normal Mesh and (c) Fine mesh

4.1.4. Boundary conditions

The inlet of the GLCC is defined as a mass flow inlet, where the mass flow rate that enters to the separator is specified and depending on the case in study is changed. The exit located at the bottom is defined as a pressure outlet. The top of the half of the GLCC and the other boundaries are defined as wall with no-slip condition.

4.1.5. CFD models

Due to the characteristics of the phenomenon in study, a three dimensional case is established with liquid as fluid with constant density. Properties of water are selected with a density of 1000 kg/m^3 and a viscosity of 1cP. A steady state model is selected since properties in the system do not have a strong variation with time. A segregated flow model is also used. This model is recommended for incompressible flows, uses less memory than the coupled flow model and it solves each momentum equation one by one with a corrector factor to link it with the continuity equation (CD-Adapco, 2016). Additionally, the gravity is enabled as it plays an important role in the separation principle of a GLCC. As the flow inside the separator is in a turbulent regime, the RANS equations and a turbulence model are required. According to the literature review, a controversy exists in the definition of the turbulence model, since the turbulence field is anisotropic as it was observed by *Erdal (2001).* For this kind of phenomenon, a Reynolds stress model should be used, but due to its complexity and extra computational load, $\kappa - \varepsilon$ turbulence model is accepted and validated by many authors. This model used two extra equations to solve taking into account a turbulent kinetic energy (κ) and turbulent dissipation rate (ε).

4.2. Two-phase flow

For the two-phase flow case, the experimental work by *Kanshio et al. (2015)* is used at first instance. For this experiment, under full separation, boundary conditions are unknown. For this reason an experimental setup was built in order to validate the model under full separation.

4.2.1. Experimental setup performed by *Kanshio et al. (2015)*

The experimental setup performed by *Kanshio et al. (2015)* was carried out in Cranfield University, UK. The considered separator did not have an inclined tangential inlet, as the described in this work. Nevertheless, the acquired data is relevant to validate multiphase simulations. The GLCC had 76.2 mm of inner diameter and 2.7 m of height. Air and water were used as fluids, an electrical resistance tomography (ERT) was located 0.2 m above the inlet, and a wire mesh sensor (WMS) in the gas outlet to measure liquid holdup.

Measurements of zero net liquid holdup under stagnant liquid and under full separation were reported. Additionally, images of phase distribution in the separator were acquired with the conductivity tomography. From this experiment, the acquired zero-net liquid holdup data will be used to validate CFD simulations. For this case, the liquid outlet was shut-off and the separator was filled with water. After that, only air enter to the system, liquid holdup was measured by ERT and reported as function inlet gas velocities. The gas velocity varies from 0.55 m/s to 10.18 m/s.

4.2.2. Experimental setup performed at Universidad de los Andes

An experimental setup is built in order to obtain data to validate the CFD model under full separation. The GLCC loop is used to gather data of the quantity of LCO and the pressure values at both outlets. Figure 7 presents a general schematic of the experimental facility.

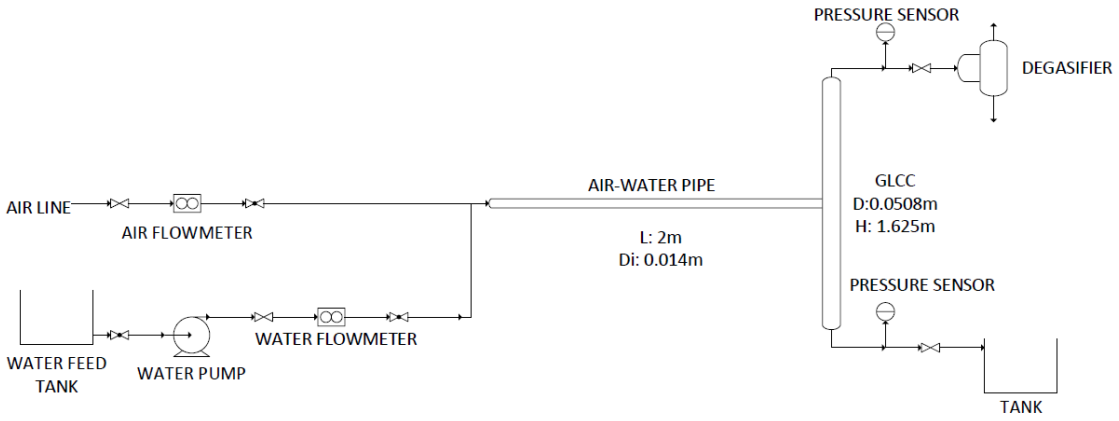

Figure 7. Schematic of the flow loop built at Universidad de los Andes

Water enters to the loop from a 200 L storage tank and passes through a Pedrollo centrifugal pump of 0.5 HP to impulse the fluid to the mixing zone. After the pump, a gate valve is used in order to regulate the flow rate and then it is measured by a Hedland water flowmeter. The range of this device is from 2 to 15 LPM. Next to the flowmeter, a globe valve is located to prevent reverse flow in the flowmeter in case of a shutdown of the system. After this metering section, water enters to a T-shape mixer, where it is combined with the air. The air comes from a pressurized line, the flow rate is regulated and measured by a Dwyer flowmeter. The range of this device is from 10 to 100 LPM. The T-shape mixer is connected to a poly methyl methacrylate pipe of 2 m of length and 14 mm of inner diameter. This pipe has 0° of inclination and is connected to the GLCC, ensuring a tangential inlet. The inlet is located at the middle height of the separator, which has a height of 162.2 m and an inner diameter of 0.0508 m. The liquid and gas leg have a Rosemount 3051 pressure transmitter in order to

define the boundary conditions in the CFD simulations. Both pressure transmitters are connected to a Keysight triple output DC power supply and programmed to work at 24 V. After the pressure transmitter, gate valves are used in order to control the liquid level and the pressure in the GLCC. The liquid leg ends in an atmospheric storage tank and water is recirculated to the feed tank. The gas leg ends in a degasifier or liquid trap, which contains a grid in the top outlet in order to avoid that small liquid droplets leaves the system with the air. In the bottom outlet of the degasifier is measured the amount of LCO. Images of the experimental setup are shown in Appendix A.

As the main goal of the experimental setup is to obtain a measurable quantity of LCO, values of superficial water velocities are defined and the superficial gas velocity is slowly increased until LCO is evidenced. In the first stages of this process, no LCO is observed, so the valve in the liquid leg is closed until this phenomenon is obtained.

4.2.3. Geometry

This section presents the proposed geometries for the two cases described before. For *Kanshio et al. (2015)* a radius of 0.0381 m is used for the GLCC body. The height above the inlet is of 1.11905 m and below the inlet is about 1.51905 m. The tangential inlet has a total length of 0.5 m and a radius of 0.0191 m. In the upper part, a conic reduction is considered with a height of 0.2 m. The small radius of this section is the same radius of the gas outlet and it measures 0.0127 m. The liquid outlet is located at the bottom and it has a radius of 0.0254 m and a length from the GLCC body of 0.1 m. The geometry for this case is shown in Figure 8 with views from different angles.

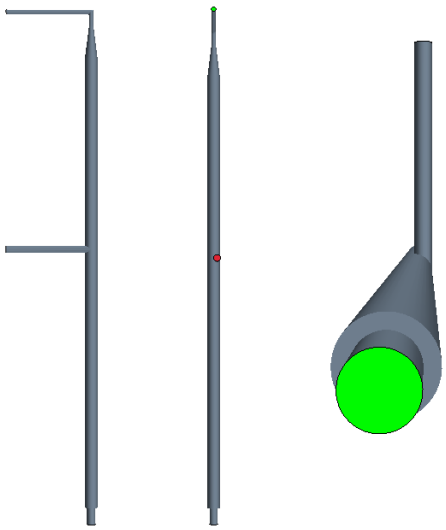

Figure 8. Lateral view, frontal view and top view of the geometry for Kanshio´s study case

For the experimental setup performed at Universidad de los Andes a GLLC with a radius of 0.0254 m and a total height of 1.625 m is proposed. The tangential inlet used includes all the air – water pipe described in section 4.2.2, from the mixing zone until the GLCC. This is done in order to define properly the boundary conditions of each phase. The radius of the gas and liquid outlet measures 0.0127 m and the length of each leg is 0.3 m. The final geometry used for this case is shown in Figure 9 from different views.

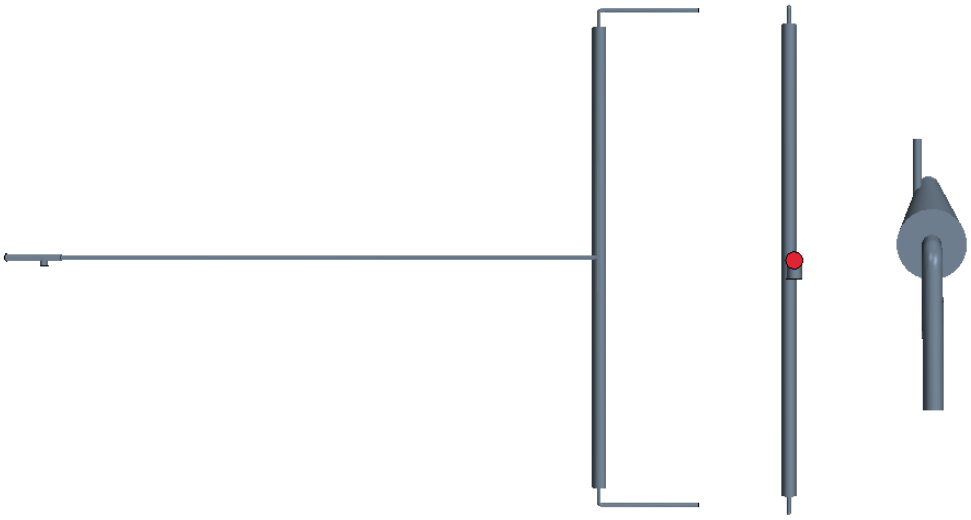

Figure 9. Lateral view, frontal view and top view of the geometry for the GLCC used at Universidad de los Andes

4.2.4. Mesh

The mesh specifications and main features are the same used for the single-phase flow case. For the case of *Kanshio et al. (2015)* three meshes are proved for the grid independence test. A coarse mesh with 247,141 cells, a normal mesh with 423,883 cells and a fine mesh with 603,783 cells, the three of them are shown in Figure 10.

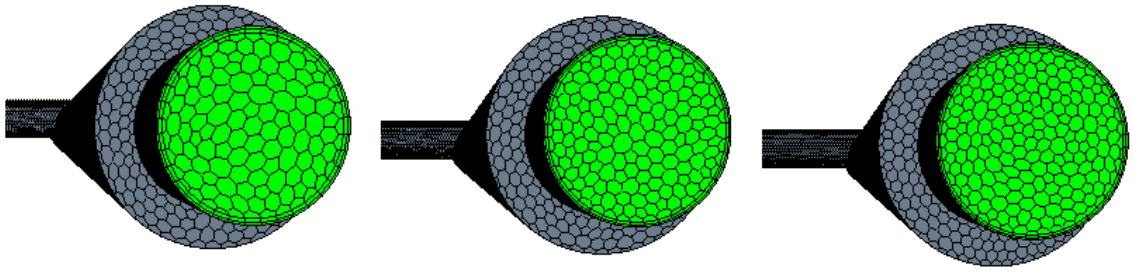

(a) (b) (c)

Figure 10. Mesh done for the grid independence test for the case of Kanshio et al. (2015): (a) Coarse mesh, (b) Normal mesh and (c) Fine mesh

For the case of the experimental setup performed at Universidad de los Andes, three meshes are proved in the grid independence test. The first one is called coarse mesh and

has 350,124 cells, the second one is called normal mesh and has 548,586 cells, and finally the third one is called fine mesh and has 680,354 cells. These meshes are shown in Figure 11.

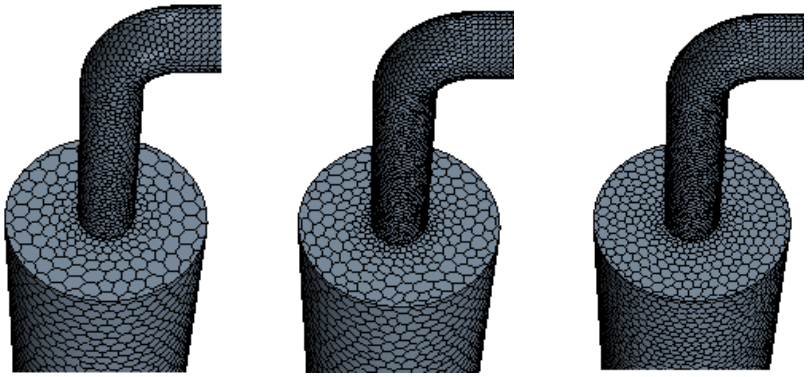

(a) (b) (c)

Figure 11. Mesh done for the grid independence test for the case of the experimental setup performed at Universidad de los Andes: (a) Coarse mesh, (b) Normal mesh and (c) Fine mesh

4.2.5. Boundary conditions

The boundary conditions are maintained equally as in the single-phase flow case. A variation can be found at the inlet, where the two phases are added, and are defined as a velocity inlet. In each phase is defined the velocity and the volume fraction. The gas outlet, which does not exists in the single-phase case, is modelled as a pressure outlet.

4.2.6. CFD models

Based on the CFD models used for the single-phase flow case, some modifications are required in order to model the two-phase flow. The implicit unsteady model is selected instead of the steady state. When this kind of model is used, it is important to assure that the Courant-Friedrich-Levy (CFL) number is below to 1 in order to obtain reliable results. This number relates the time-step, the velocity and the space between cells. Additionally, the Volume of Fluid (VOF) is used as multiphase model. This model is considered under the Eulerian description, which is the most common mathematical model used to describe a multiphase flow. It consists on the recording of the evolution of flow properties at fixed points in the geometry domain as time varies. The Eulerian description is used mainly in Fluid Mechanics for the reason that mathematically is simpler to apply (Deparment of Ocean Engineering, MIT, 2011). The VOF model is used for immiscible fluids and to track the interphase between them. The model assumes that both phases share pressure and velocity fields, so it only uses a single set of momentum and mass equations. An important parameter to be considered is the volume fraction which describes the spatial distribution of

a phase (CD-Adapco, 2016). The equations that describes the VOF model are shown in equations 8 to 11.

$$\rho = \sum_i \rho_i \alpha_i \tag{8}$$

$$\mu = \sum_i \mu_i \alpha_i \tag{9}$$

$$\alpha_i = \frac{V_i}{V} \tag{10}$$

$$\frac{d}{dt}\int_V \alpha_i dV + \int_S \alpha_i (v - v_g) \cdot da = \int_V \left(s_{\alpha_i} - \frac{\alpha_i}{\rho_i}\frac{D\rho_i}{Dt} \right) dV \tag{11}$$

From previous equations sub index i represents the i^{th} phase, ρ the density, μ the viscosity, α the volume fraction. An important parameter in the settings of this model is called the sharpening factor, which is defined between zero and one and is related with numerical diffusion. Zero is the default value and do not reduces the numerical diffusion, but is enough for many cases. The value of one implies that there is not numerical diffusion, but convergence problems could appear (CD-Adapco, 2016). If a value different from zero is used, an additional term is added to equation 11.

4.3. Geometry modifications of the GLCC

Five geometry variables are evaluated, and the descriptions are presented in this section. Those variables are: (i) Inclination angle of the tangential inlet. (ii) The height of the tangential inlet. (iii) The effect of including a dual inlet. (iv) The influence of including a nozzle or reduction in area at the inlet of the GLCC. (v) The effect of including a volute inlet with rectangular slot. Using the same conditions of the experimental base case, all the proposed modification are simulated in STAR-CCM+ with the same CFD model. The comparison of all cases is done with the amount of LCO and GCU.

4.3.1. Inclination angle of the tangential inlet

As it can be seen in the literature review, most of the GLCC uses an inlet with an inclination angle of 27°. In order to observe if this angle has a better performance than the inlet with no inclination, and to analyze the effect of this variable, five levels are selected to simulate the GLCC and are shown in Figure 12. The length of the section that is inclined is of 15 cm.

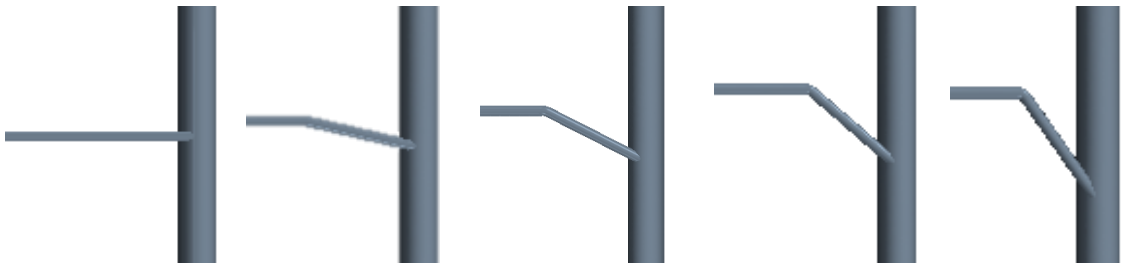

Figure 12. Evaluated inclination angles of the tangential inlet: (a) 0°, (b) 13°, (c) 27°, (d) 41° and (e) 55°

4.3.2. Height of the tangential inlet

Traditional GLCC has located the tangential inlet around the center of the total height. In this study, the effect of moving the inlet upward and downward is analyzed for horizontal inlet. For this reason, 4 levels are selected in this variable and are shown in Figure 13.

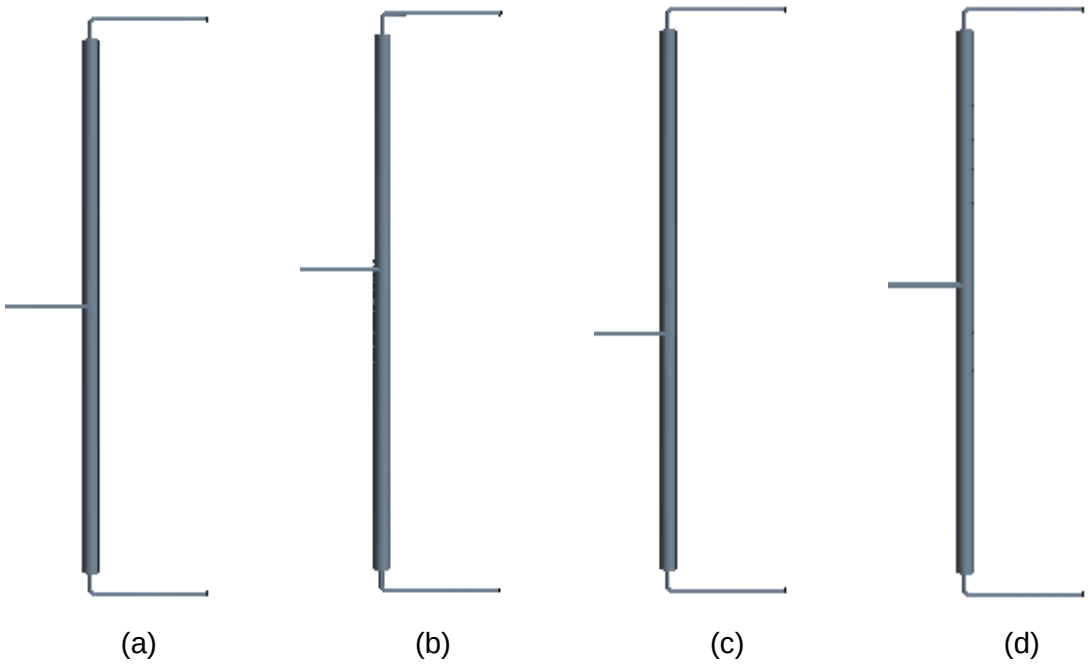

Figure 13. Evaluated heights of the tangential inlet: (a) Center, (b) 10 cm above center, (c) 10 cm below center and (d) 5 cm above center

4.3.3. Dual Inlet

In the literature review, as in *Gomez (2001)*, was found the use of a dual inlet in order to have a pre-separation of liquid and gas phases and slug handling. To analyze the effect of this geometrical modification, three cases are evaluated varying the distance between both inlets and are shown in Figure 14. The length of the upper inlet is of 30 cm.

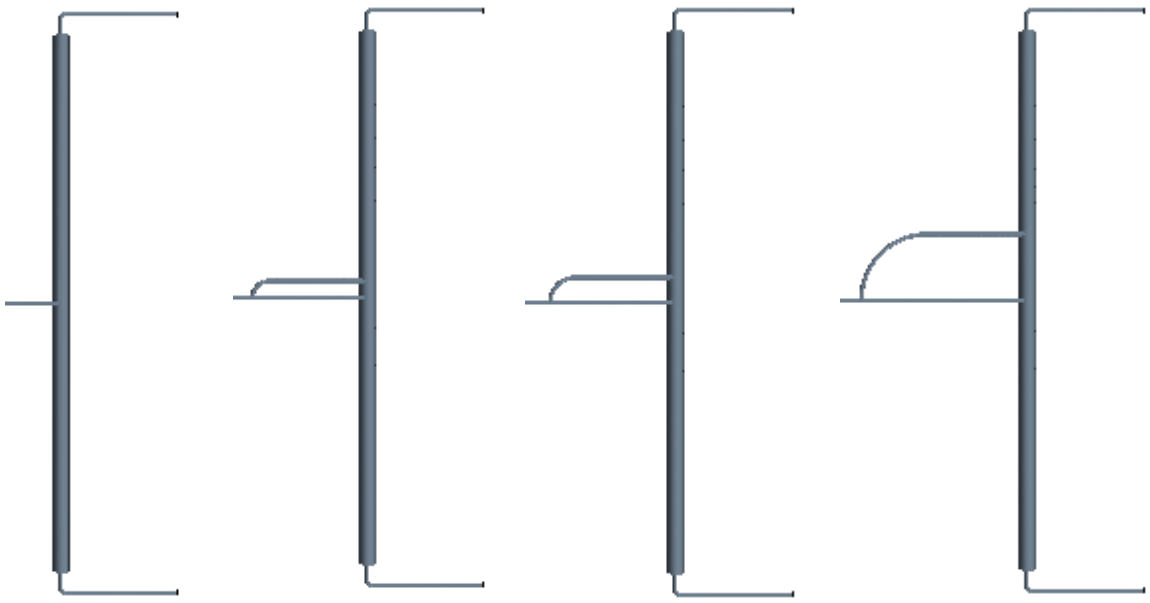

(a) (b) (c) (d)

Figure 14. Evaluated configurations for dual inlets: (a) Single inlet, (b) Dual inlet with 5 cm between both inlets, (c) Dual inlet with 7.5 cm between both inlets and (d) Dual inlet with 20 cm between both inlets

4.3.4. Nozzle

Including a nozzle or an area reduction could be helpful to the separation process, due to the fact that it rises the velocity and the centrifugal force inside the GLCC. For this reason, four levels are evaluated in this variable and its configurations are shown in Figure 15. The length of the section that presents an area change is of 5 cm.

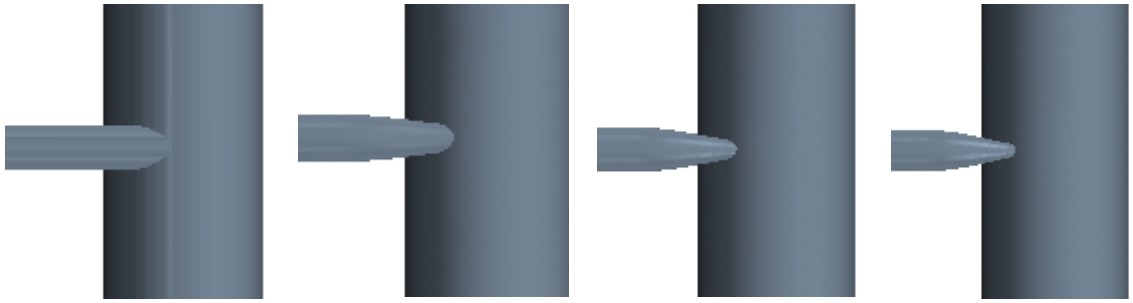

(a) (b) (c) (d)

Figure 15. Evaluated nozzle configurations: (a) Without nozzle, (b) Nozzle of 7 mm of diameter, (c) Nozzle of 3.5 mm of diameter and (d) Nozzle of 1.75mm of diameter

4.3.5. Volute inlet with rectangular slot

In the same order of ideas as in the nozzle, an area reduction is evaluated including a volute inlet with rectangular slot. For this variable, five levels are simulated and are shown in Figure 16. The length of the section that presents an area change is of 5 cm.

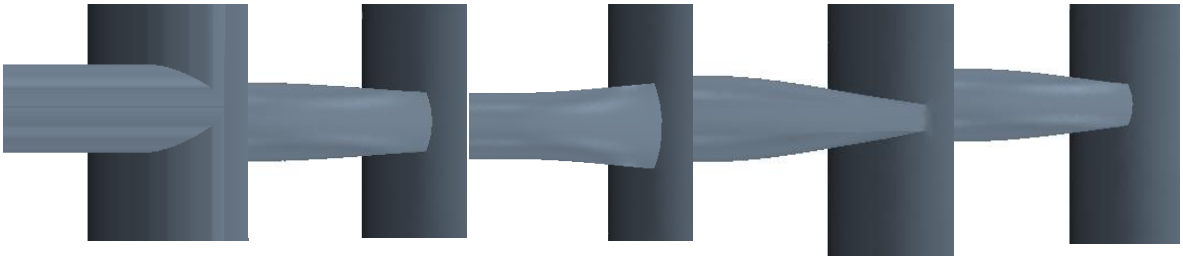

Figure 16. Evaluated configurations of the volute inlet with rectangular slot: (a) Without volute inlet, (b) Volute inlet of 25% of pipe area (9.62 mm of height and 4 mm of width), (c) Volute inlet of 25% of pipe area (19.24 mm of height and 2 mm of width), (d) Volute inlet of 25% of pipe area (4 mm of height and 9.62 mm of width) and (e) Volute inlet of 15% of pipe area (6.597 mm of height and 3.5 mm of width)

5. Results

In this section, the results obtained in STAR-CCM+ for the different cases are presented, as well as the experimental results.

5.1. Single-phase flow – swirling flow validation

The case of 0.00454 m^3/s of water is used for the grid independence test. The results for the three meshes are compared with experimental data of tangential velocities and are shown in Figure 17.

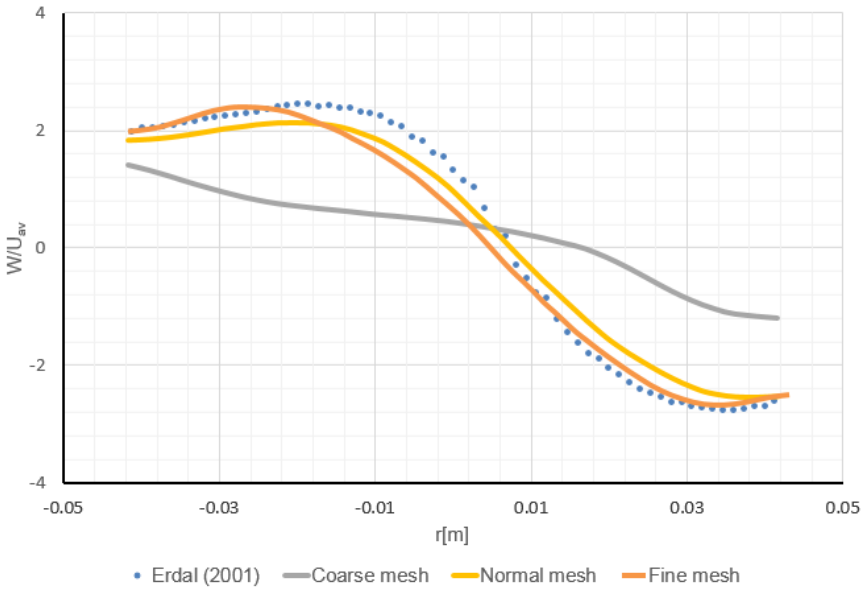

Figure 17. Results for the grid independence test for the case of 0.00454 m^3/s

From Figure 17, it can be seen that the results of the coarse mesh differ from the experimental data, while the normal mesh and the fine mesh describes the behavior of the experimental results. Comparing the normal and fine mesh, there is not a considerable difference, but at the lowest and highest radius the fine mesh fits better the measured values. However, the normal mesh is selected for the reason that it requires less computational time to find a solution, and the results do not have a considerable difference as compare with the with the fine mesh.

Once the mesh size is selected, different cases are simulated following the experimental matrix reported by *Erdal (2001)*. In this document only the results for the case of 0.00454 m^3/s of water are presented. In Figure 18 a comparison between the tangential velocities profiles obtained experimentally by *Erdal (2001)* and the CFD profiles are shown at three different heights below the inlet.

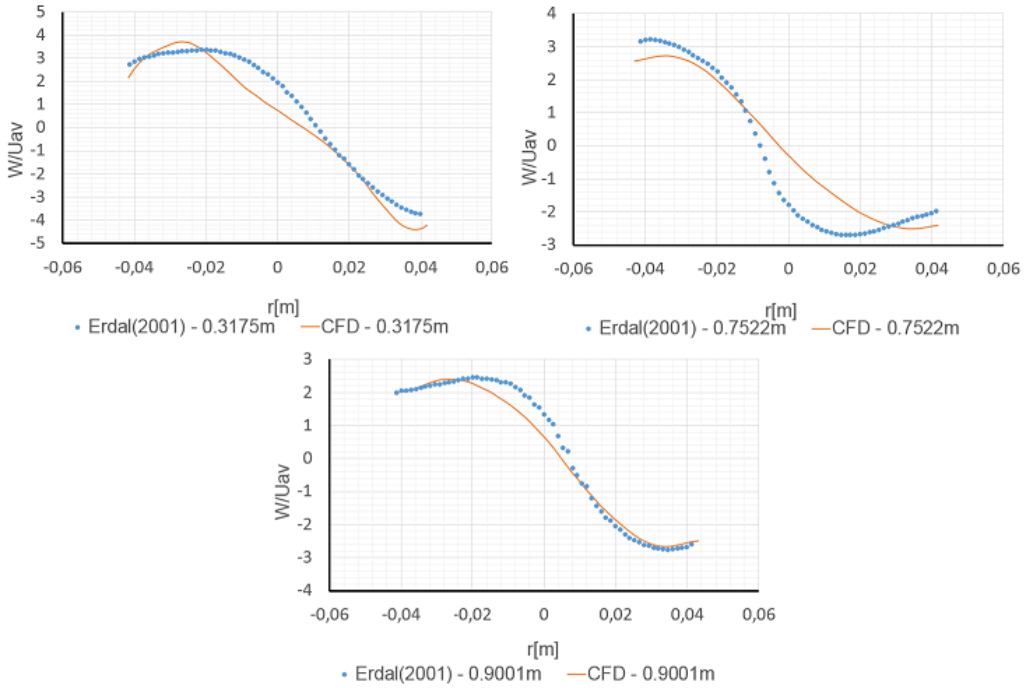

Figure 18. Results for tangential velocity at three different altitudes: (i) 0.3175m (ii) 0.7522m and (iii) 0.9001m

The CFD results seems to describe the behavior achieved experimentally and for fully developed flow at the lowest measure point, simulation results tend to fit better the experimental data. The corresponding Root Mean Square (RMS) error for each case is 74%, 80% and 37%, respectively. In Figure 19 similar comparison is presented but considering the axial velocities profiles.

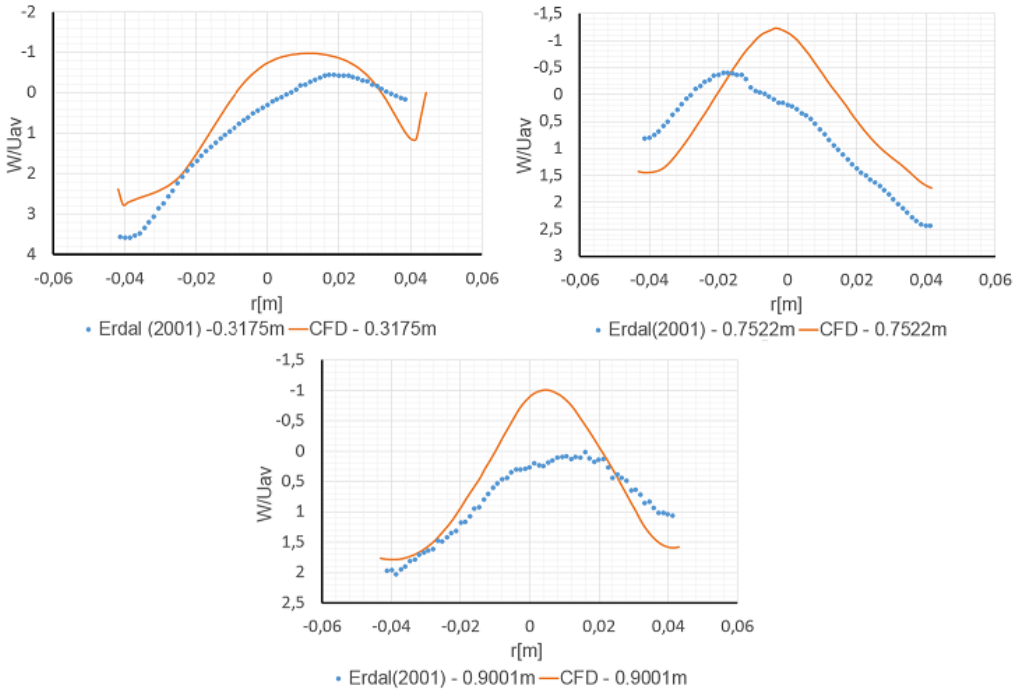

Figure 19. Results for axial velocity at three different altitudes: (i) 0.3175m (ii) 0.7522m and (iii) 0.9001m

From Figure 19, it is clear that axial velocities profiles differ more to the experimental data than the tangential velocity profiles. The corresponding RMS error for each case is 75%, 90% and 58%, respectively. The main objective of the single-phase case is to validate the capability of CFD to represent the vortex inside the cyclone. An evidence that this is achieved can be seen in Figure 20, where the vortex is clearly observed at the center of the GLCC.

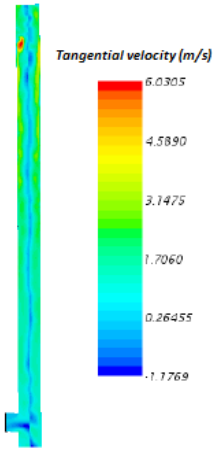

Figure 20. Tangential velocity profile

5.2. Two-phase flow – zero net liquid flow

The case of a superficial gas velocity of 0.55 m/s in *Kanshio et al. (2015)* is used for the grid independence test and to compare the effect of the sharpening factor. After trial and error process, a total time of 25 seconds is recommended for all cases owing to that there is not variation on the results and the volume fraction of air at the top outlet remains constant (near to 1). The results obtained presents oscillations and noise as it can be seen in Figure 21, where the liquid holdup at the location of the ERT measures is plotted against time for a coarse mesh. In order to visualize better the results and to compare them, a linear regression is plotted in Figure 21.

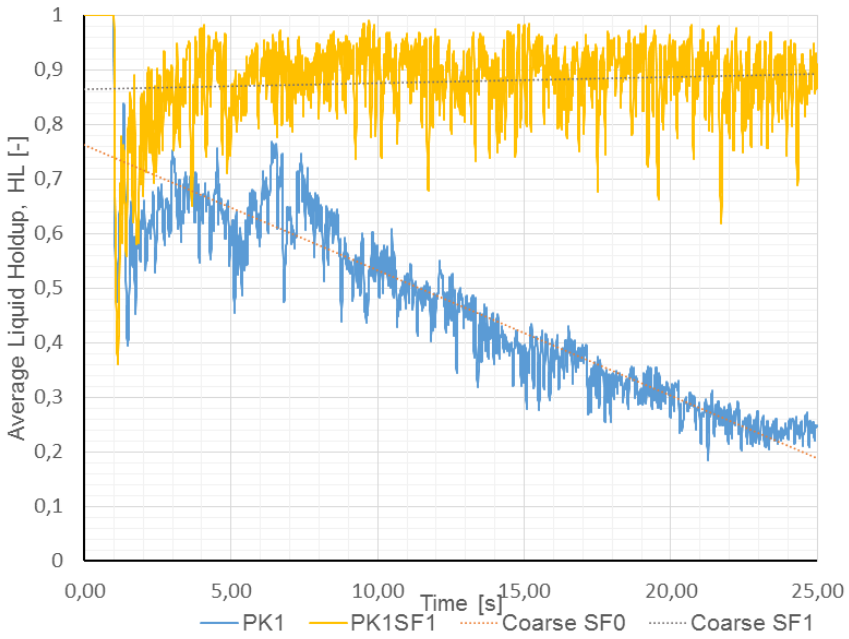

Figure 21. Results obtained for a coarse mesh and an inlet gas velocity of 0.55 m/s

As it can be seen from Figure 21, the linear regression describes the behavior of the results. Therefore, in Figure 22 are compared the results obtained for the three meshes and each one for a sharpening factor of 0 and 1. The experimental value reported for this case is 0.8. In order to obtain a value from the simulation and to avoid the noise of the results, an average of the last five seconds is used.

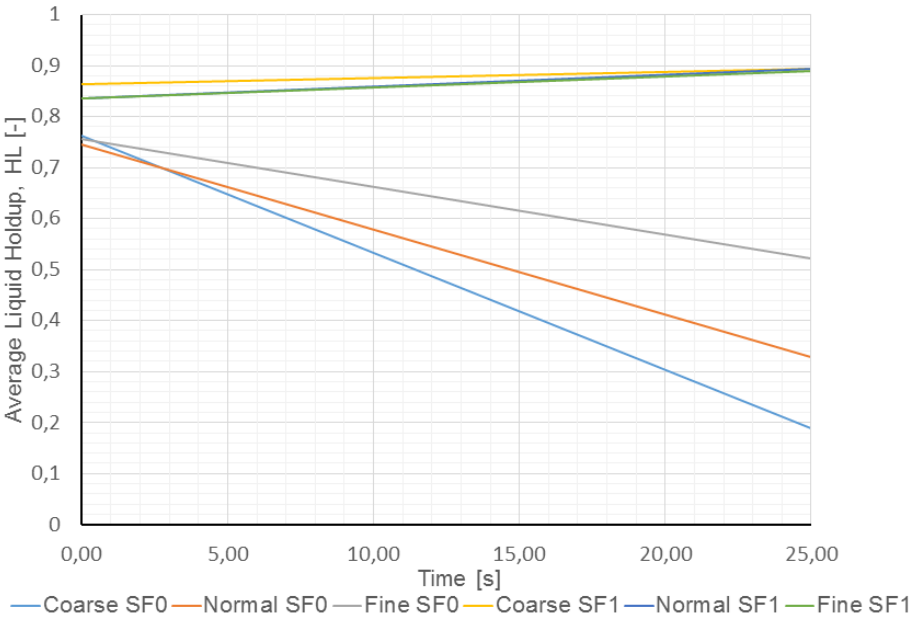

Figure 22. Results for the grid independence test and the comparison of the results using a sharpening factor of 0 and 1

From Figure 22, it is observed that there is a big difference between the results obtained with the sharpening factor of 0 and 1. Additionally, the value of the liquid holdup at the end of the time is near to the experimental value when the sharpening factor was defined as 1. For this reason, and to complete the experimental curve, this value is selected for the rest of the simulations. Analyzing the effect of the mesh in the results, it can be seen that for a sharpening factor of 0 results are dependent on the mesh, while for a value of 1 there is only a slight discrepancy for the first 15 seconds, following the same behavior afterwards. Analyzing only in the results for a sharpening factor of 1, the normal mesh is selected for the reason that the coarse mesh has the biggest difference in the first 15 seconds and there is not a considerable difference requiring less computational time as compare with the fine mesh. It is important to notice that in order to assure the condition of the CFL number, different time-steps are used for each evaluated mesh. Once the mesh and the sharpening factor are defined, simulations to obtain the results for the whole zero-net liquid holdup under stagnant liquid condition can be executed. The results from these CFD simulations and its comparison with the experimental data are shown in Figure 23.

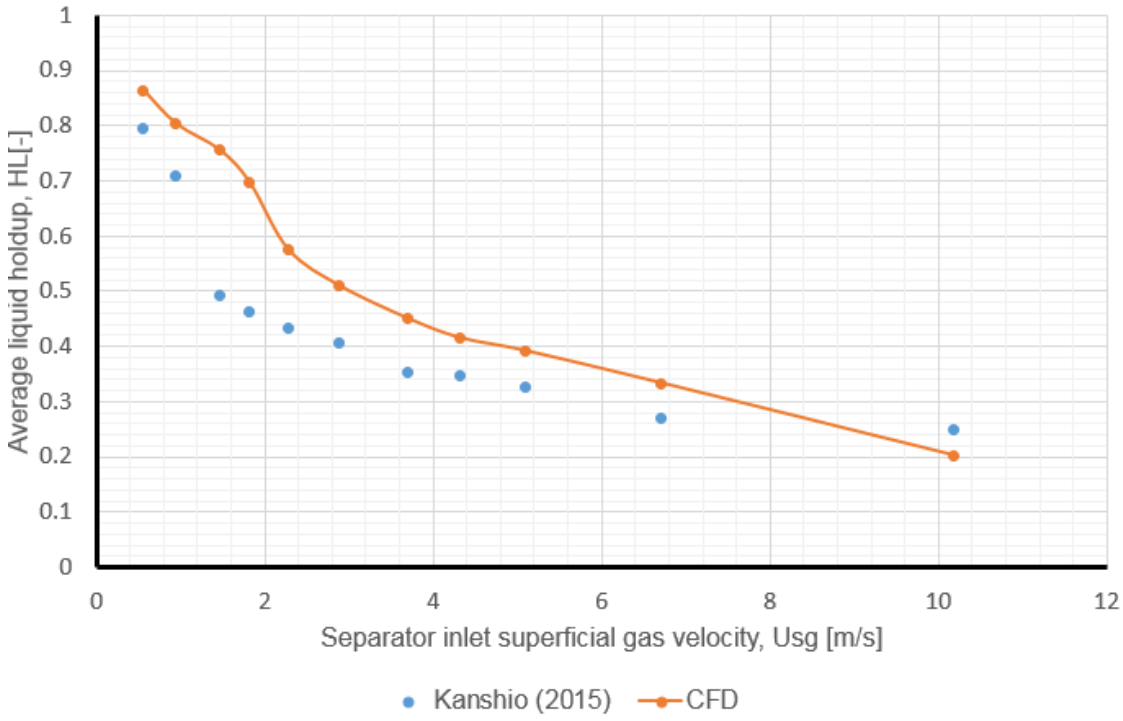

Figure 23. Results for liquid holdup under zero-net liquid flow

From Figure 23, it can be observed that the CFD results describes the behavior reported in the experimental study; when the superficial gas velocity at the inlet increases, the average liquid holdup at the measure point decreases as more liquid is blown out by the gas. The

RMS error obtained between the CFD results and the experimental values is about 13%, which implies a fair agreement. *Kanshio et al. (2015)* describes the flow of liquid above the inlet as “the remaining liquid in the separator kept rising and falling in a chaotic manner similar to typical churn flow” (Kanshio et al., 2015). This observation is reproduce as well by CFD as it is shown in Figure 24 by a scalar field of the volume fraction of air through a plane and by streamlines.

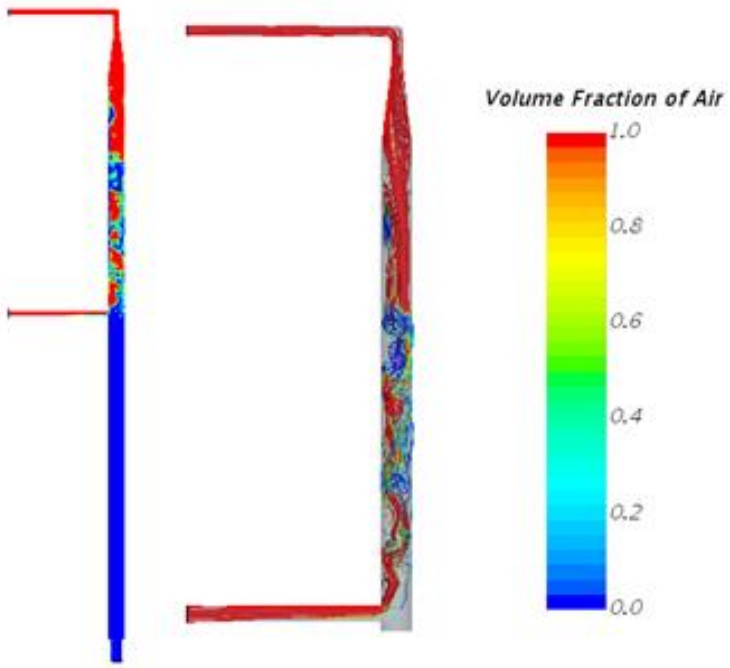

Figure 24. Scalar field of the volume fraction of air and streamlines from the CFD results

5.3. Two-phase flow – both phases entering into the GLCC

This section is divided into four parts. The first one shows the results obtained from the experimental setup. The second one is the validation in STAR-CCM+ of a selected experimental case. The third one is the evaluation of the proposed geometrical modifications by CFD simulations. Finally, the fourth one is the analysis of the swirling flow decaying into pipe flow using the CFD software.

5.3.1. Experimental results

The case with a gas flow rate of 40 LPM and water flow rate of 13 LPM is selected as the base case for this analysis. This case is chosen for the experimental procedure and for the CFD methodology. This case is selected due to the fact that with this conditions a measurable amount of LCO is obtained. In Table 4 can be found the results for the experimental procedure.

Table 4. Experimental results of the selected case

$Q_G(LPM)$	$Q_L(LPM)$	Pressure top outlet (psi)	Pressure bottom outlet (psi)	LCO (mL/s)
40	13	10.79	12.35	3.12
40	13	10.80	12.45	5.88
40	13	10.80	12.42	5.89
40	13	10.80	12.50	10.73
40	13	10.80	12.45	4.75
40	13	10.80	12.38	3.06
40	13	10.80	12.46	7.46
40	13	10.80	12.41	6.02
40	13	10.80	12.43	5.71

From Table 4 it can be observed that the pressure at the top outlet is the atmospheric and no significant variation is evidenced. The pressure at the bottom outlet is higher than the pressure at the top outlet. It is expected due to the fact that the valve located in the liquid leg is closed in a high percentage and there is a liquid column in the separator that increases the pressure value. The observed range varies from 12.35 to 12.50 psi and a major variation is observed in this outlet. In all cases LCO is evidenced. The data is acquired since the first time an amount of liquid is observed in the top outlet. The quantity of water is recollected for more than 30 seconds and measured. It can be observed that the amount of LCO presents variations between runs, and a small difference in the pressure value in the liquid exit indicates a change in the LCO. For most cases, when the pressure at the bottom increases, a higher amount of LCO is obtained. This is due to the fact that at higher values, water founds more resistance to leave the GLCC, then the separator fills more with water, and the flow rate of water at the top exit increases.

5.3.2. Validation of the CFD model

In order to validate the experimental results with STAR-CCM+ a fix value of the pressure at bottom outlet must be selected, and a fix value of the amount of LCO should be used for comparison. The value used for pressure is 12.425 psi, which is the middle value of the range of the obtained data, and is very near to the average (12.428 psi). The selected value for the LCO is the average of the reported data, which is 5.85 mL/s. A total time of 85 s is simulated and the results are obtained from the last 30 s of the simulation.

In order to validate the results a grid independence test is done with three different sizes. The results obtained with each mesh and its comparison with the experimental results are shown in Table 5.

Table 5. Results of the validation of the CFD model using different mesh sizes

	Coarse mesh	Normal mesh	Fine mesh
LCO (mL/s)	8.22	7.22	5.50
Error (%)	40.51	23.42	5.98

From Table 5 it can be seen that the mesh has a direct effect on the results, and the mesh that presents the minor error is the fine mesh with only 5.98%. This indicates that the CFD model is capable to represent the different phenomena that occurs during the operation of a GLCC. Otherwise, the difference in computational time between the different meshes is high. For this reason and as many cases are proved in this study, the selected size to evaluate the geometrical modifications is the normal mesh.

5.3.3. Evaluation of geometrical modifications

Once the CFD model is validated with the experimental results and a mesh size is selected, the simulations of all the proposed geometrical modifications are evaluated. The first variable that is analyzed is the inclination angle of the tangential inlet. The results for LCO and GCU for the five selected levels are shown in Figure 25.

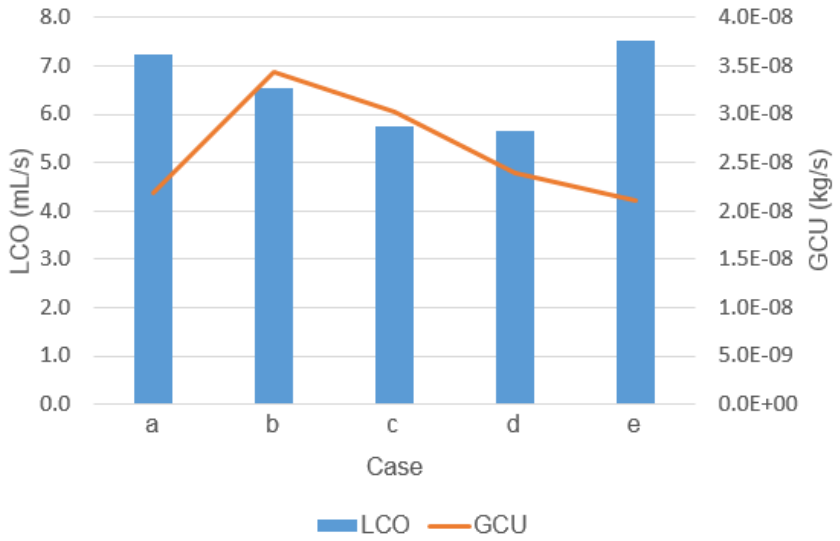

Figure 25. LCO and GCU results for the evaluated inclination angles of the tangential inlet: (a) 0°, (b) 13°, (c) 27°, (d) 41° and (e) 55°

From Figure 25 it can be observed that the LCO obtained experimentally, with no inclination in the inlet, can be reduced using a certain inclination angle. Values of 13°, 27° and 41° show an improvement, while an angle of 55° presents a higher amount LCO. This indicates that there is an optimal angle that produce the minimum LCO. For 27° and 41° the LCO presents the lower values, but with not a significant difference between them. *Kouba et al (1996)* established that an inclined inlet reduces LCO at moderate to high gas velocities,

and suggest that a value of 27° should be adequate. The two main reasons are that when the inlet presents an inclination, a stratification in gas and liquid phase is favored, which represents a pre-separation, and that with this configuration liquid enter below the inlet and a blocking of gas is avoided (Kouba et al, 1996). Most of reported GLCC with an inclined tangential inlet used an angle of 27° (Movafaghian, 1997; Erdal, 2001; Gomez, 2001; Guzmán, 2005; Hreiz et al., 2013).

Analyzing the results for the GCU, it can be seen variations between the different angles. For 13° 27° and 41° a higher value of GCU is obtained than in the case with 0°. When the angle increases, the GCU seems to decrease, but the magnitude order is too small in all cases that it is negligible in comparison to the amount of air that is entering to the GLCC (about a 0.0003%). Moreover, is negligible comparing the volumetric flow at the bottom outlet as it represents less than the 0.00013%. In this order of ideas, taking into account the results for LCO and the literature review, 27° seems to be an adequate angle to reduce LCO in a GLCC.

The second variable that is analyzed is the height of the tangential inlet. The results for LCO and GCU for the four levels evaluated in this case are shown in Figure 26.

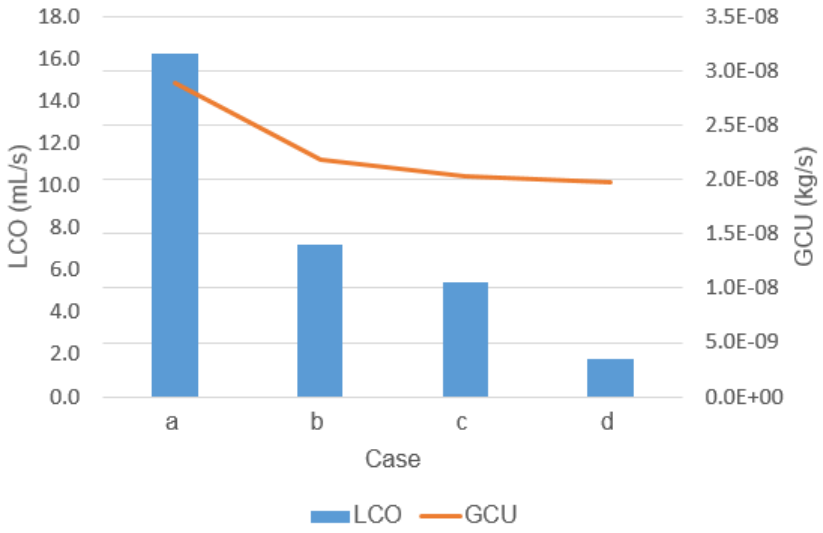

Figure 26. LCO and GCU results for the evaluated heights of the tangential inlet: (a) 10 cm below center, (b) Center, (c) 5 cm above center and (d) 10 cm above center

From Figure 26 it can be seen that height of the inlet has a big effect in the amount of LCO, and seems to have a stronger impact than the inclination angle of the tangential inlet. When the inlet is located 10 cm above the center, the amount of LCO reduces considerably. Opposite situation occurs when the inlet is placed 10 cm below the center. An intermediate case is evaluated using an inlet located 5 cm above the center of the GLCC. For this case,

a reduction in LCO is observed when it is compared with the original case, but it is not good as the inlet placed 10 cm above the center. In literature, *Shoham (1998)* stated that the inlet should be located above the liquid level of the GLCC and recommended values for liquid level between 1 to 3 L/D below the inlet. Unfortunately, in this case the liquid level could not be determined experimentally for the reason that the GLCC is not transparent and no liquid level sensor has been installed. At the selected case, the GLCC is flooded by liquid, so the liquid level is too high and increasing the height of the location of the tangential inlet will reduce the amount of LCO. The obtained results agree with the experimental setup performed by *Movafaghian (2000)* and *Hreiz (2014)* in which the inlet is placed a certain distance above the center of the GLCC. On the other hand, the GCU in this variable presents a direct relationship with the LCO, this means when the amount of LCO is reduced, the amount of GCU reduces as well and vice versa. As in the previous case, the amount of GCU is negligible. Considering the obtained results and the described literature review, the best of the evaluated location of the tangential inlet is 10 cm above the center.

The third variable that is evaluated is the use of a dual inlet. The results of LCO and GCU for the four levels used in this variable are shown in Figure 27.

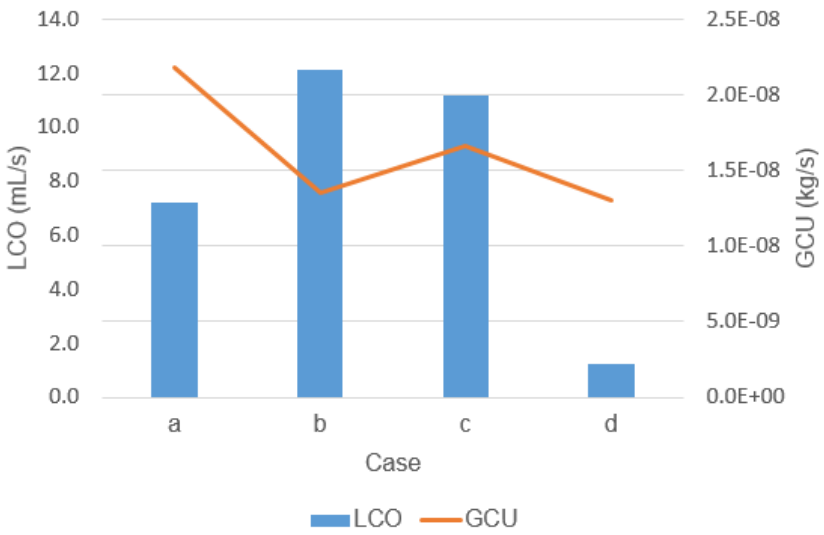

Figure 27. LCO and GCU results for the evaluated configurations for dual inlets: (a) Single inlet, (b) Dual inlet with 5 cm between both inlets, (c) Dual inlet with 7.5 cm between both inlets and (d) Dual inlet with 20 cm between both inlets

From Figure 27 it can be observed that a dual inlet must to be used carefully since in two cases an increase in the amount of LCO is observed. For this particular case, a direct relationship between the separation of both inlets and the reduction of LCO is evidenced. When the inlets are separated by 5 cm and by 7.5 cm the LCO increases comparing with a

single inlet, but when this distance increases to 20 cm a clear reduction of this phenomenon is observed. *Movafaghian (1997)* tested experimentally the use of a dual inlet and founds that for low to moderate superficial velocities of gas the dual inlet is much better than single inlet. It is related with the flow pattern at the inlet, at low velocities of gas, segregated flow pattern or slug flow is obtained and the dual inlet can pre-separate both phases, while with high superficial gas velocities annular flow pattern is obtained and the pre-separation is limited. In the experimental setup, as the inlet is transparent it is observed the water at the bottom of the pipe and gas in the upper part. This behavior is obtained in the CFD simulations at it can be found in Appendix B. As the gas is transported in the upper zone of the pipe, the majority of this phase must go in the upper inlet, while a rich flow in liquid must go in the lower inlet. One may concern is exposed by *Kanshio (2015)* who said that "the major challenge is where to locate the upper branch" (Kanshio, 2015). This is evaluated with the CFD simulations and for this case the biggest distance between inlets obtain the smallest LCO. When the distance is too small, both phases are entering the GLCC in the same zone and the effect of the pre-separation is lost. Additionally, the increase in LCO for the distance between inlets of 5 cm and 7.5 cm could be explained since gas is entering into a region where liquid is present and is dragging it to the top outlet. Observing the results of GCU, for all cases of the dual inlet, a reduction is obtained, in part due to the pre-separation done by the inlets. As in the previous two geometrical variables, the value of GCU is negligible.

The fourth variable that is analyzed is the use of a nozzle. Results for LCO and GCU for the four levels evaluated in this variable are shown in Figure 28.

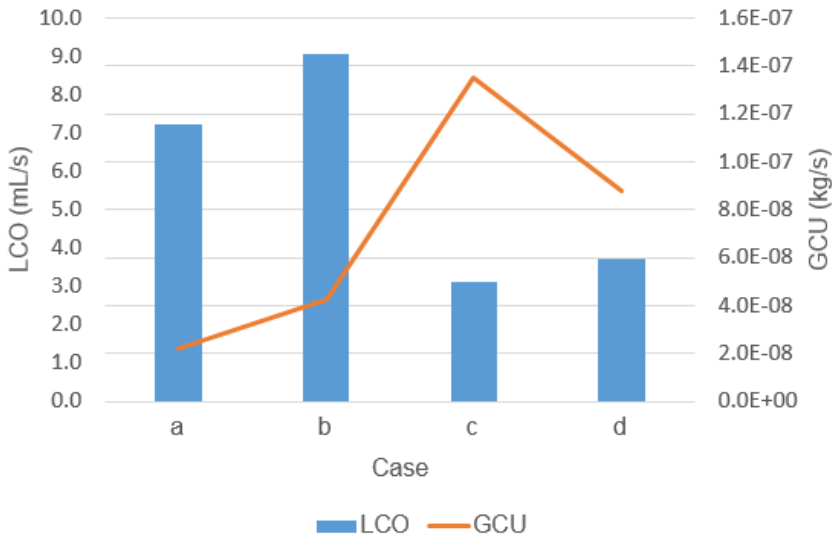

Figure 28. LCO and GCU results for the evaluated nozzle configurations: (a) Without nozzle, (b) Nozzle of 7 mm of diameter, (c) Nozzle of 3.5 mm of diameter and (d) Nozzle of 1.75mm of diameter

From Figure 28 it can be observed that the reduction of area to increase the velocity with a nozzle has a direct effect on the amount of LCO and GCU. When the area is half of original (nozzle with 7 mm of diameter) an increase in LCO is obtained, but when the reduction in area is bigger, a positive effect is evidenced. The case of a nozzle with 3.5 mm of diameter, that represents an area of 25% of the original, is the one that reduces more the amount of LCO. The nozzle of 1.75 mm of diameter, reduces as well LCO, but not as much as the previous case. In this order of ideas, it can be seen that the dimensions of the nozzle must to be selected carefully in order to reduce the LCO in the GLCC. *Hreiz et al. (2013)* studied experimentally the use of three different nozzles in the GLCC. They found that for some nozzles the swirling flow was increased and the separation enhanced, reducing the LCO, but with other kind of nozzle, when the swirl intensity was too high a short-circuiting was evidenced. The obtained results are in concordance with these experimental results and could explain why the highest area reduction does not obtain the best results. Analyzing the GCU, for cases with considerable amounts this phenomenon, the use of a nozzle could present problems for the reason that in all evaluated cases, an increase in the amount of GCU is evidenced and the higher order of magnitude is obtained for all the geometrical variations evaluated. Nevertheless, the amount of GCU continues to be negligible since it represents less than the 0.002% of the gas that is entering into the GLCC.

The fifth variable that is analyzed is the use of a volute inlet with rectangular slot. The results for LCO and GCU of the five levels evaluated in this case are shown in Figure 29.

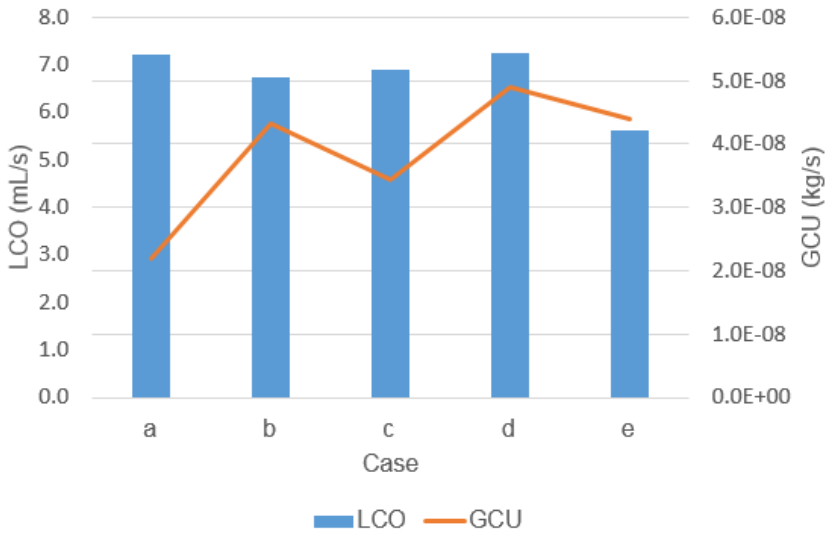

Figure 29. LCO and GCU results for the evaluated configurations of the volute inlet with rectangular slot: (a) Without volute inlet, (b) Volute inlet of 25% of pipe area (9.62 mm of height and 4 mm of width), (c) Volute inlet of 25% of pipe area (19.24 mm of height and 2 mm of width), (d) Volute inlet of 25% of pipe area (4 mm of height and 9.62 mm of width) and (e) Volute inlet of 15% of pipe area (6.597 mm of height and 3.5 mm of width)

From Figure 29 it is observed that difference between cases of an area of 25% pipe area and the original case is very small in terms of LCO. From these three cases, it is proved three dimensions of the rectangular slot of the volute inlet, and the best result is obtained with 9.62 mm of height and 4mm of width. In addition, a reduction of the pipe area to a 15% is proved and the results are better that previous analyzed case. As this geometrical modification represents an area reduction as in the nozzle, it is suitable to compare both results. It is clear that the configuration of the nozzle is better to reduce the LCO than the rectangular volute inlet for the reason that for the same area, the results of the nozzle reduce much more the amount of LCO. In addition, as it happens with the nozzle, the GCU increases in all cases with the volute inlet and continues to be negligible. *Adebare (2006)* proved three rectangular slots with different areas in a GLCC and concluded that the area variation of this slots at the inlet had a negligible effect on the LCO. The results obtained in CFD simulations agree with *Adebare (2006)* since a very light improvement is observed with the use of a rectangular slot.

Finally, a case that combines the best level of the evaluated geometrical variables is done in order to see the effect on the LCO. This case uses an inclination angle of the tangential inlet of 27°, uses a dual inlet in which the lower inlet is placed 10 cm above the center, the distance between inlets is of 20 cm, and the lower inlet has a nozzle of 3.5 cm of diameter. The geometry that represent this case is shown in Figure 30.

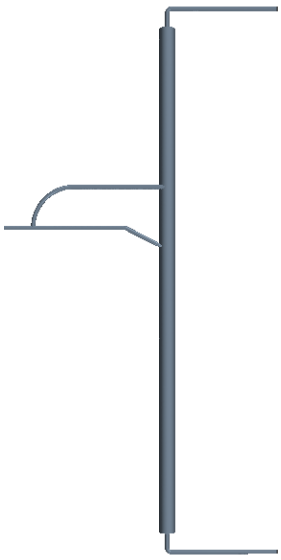

Figure 30. Geometry for the case that combines the best option of the geometrical variables evaluated

The value of LCO obtained for this case is of 0.14 mL/s which represents a reduction of 98% from the original case. In this order of ideas, the combination of the geometrical variables

analyzed enhance the performance of the GLCC and seems to be a recommendable configuration for cases with LCO. The value of GCU is 1.47x10^{-8} kg/s, which continues in the same order of magnitude of the other cases and represents a negligible value.

5.3.4. Swirling flow decaying into pipe flow

The swirl flow inside the GLCC is studied for four cases with low inlet velocities of air and water and are related with the Reynolds number. *Abdelsalam et al. (2016)* define the Reynolds number for a mixture of gas-liquid as it is shown in equation 12.

$$Re_M = \frac{\rho_L (V_{sL} + V_{sG}) D}{\mu_L} \tag{12}$$

Where ρ_L is the liquid density, V_{sL} is the superficial liquid velocity, V_{sG} is the superficial gas velocity, D is the pipe diameter and μ_L the liquid viscosity.

The first case has superficial inlet velocities of 0.66 m/s and 0.066 m/s for air and water, respectively. With these values, the Reynolds number of the mixture in the inlet pipe is 11,372. In Figure 31 vector plots of velocity are shown in six different planes below the inlet in order to visualize the swirling flow.

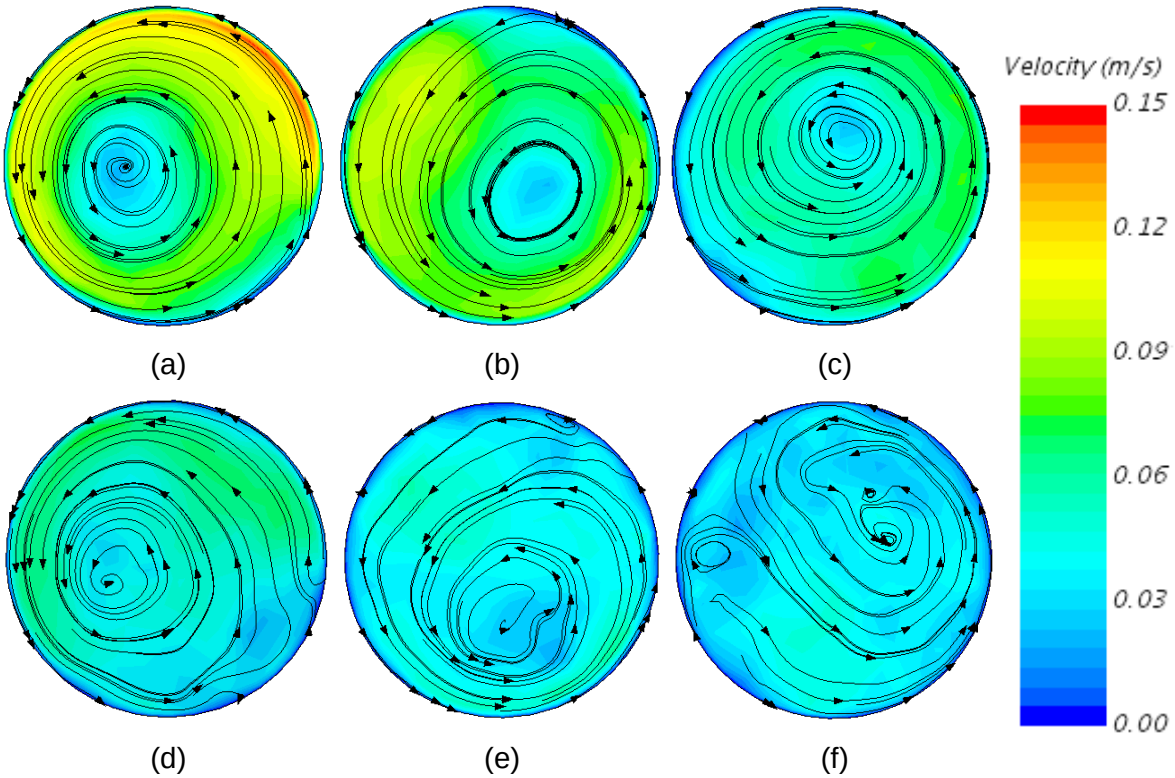

Figure 31. Swirling flow in the GLCC visualized in velocity vector plots at planes below the inlet located at (a) -5 cm (b) -10 cm (c) -15 cm (d) -20 cm (e) -25 cm and (f) -30 cm, for inlet velocities of $V_{sG} = 0.66\ m/s$ and $V_{sL} = 0.066\ m/s$

From Figure 31 it can be seen that the swirl intensity is decreasing in lower regions of the GLCC, and in the plane located 30 cm below the inlet the swirl flow is very weak. A reduction of inlet superficial velocities is proved in a second case in order to observe what happens with the swirl inside the GLCC. Figure 32 shows the velocity vector plots at different planes below the inlet for inlet superficial velocities of 0.33 m/s and 0.033 m/s for air and water, respectively.

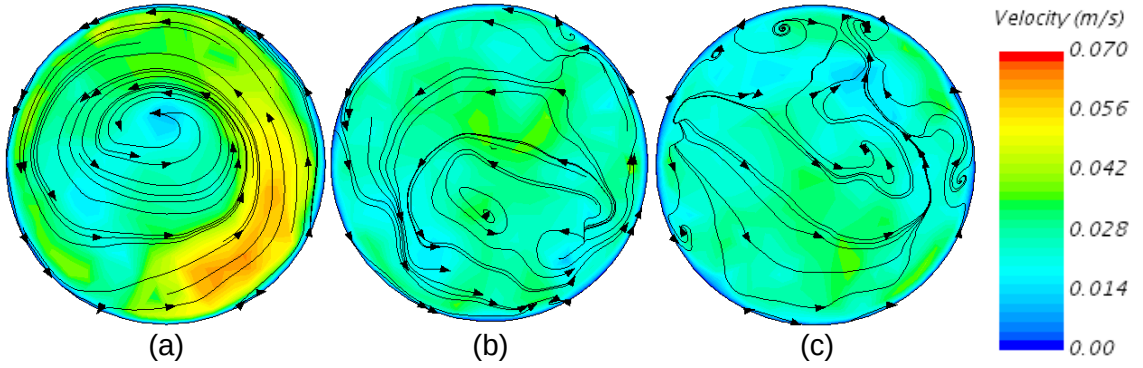

Figure 32. Swirling flow in the GLCC visualized in velocity vector plots at planes below the inlet located at (a) -5 cm (b) -10 cm (c) -15 cm, for inlet velocities of $V_{sG} = 0.33\ m/s$ *and* $V_{sL} = 0.033\ m/s$

From Figure 32 it is observed that the swirl presents lower velocities than in the previous case and at 15 cm below the inlet no swirl is evidenced. For this case the Reynolds number for the mixture in the inlet pipe is half of the previous case, it means 5,686. As in the previous two cases the gas velocity is higher than liquid velocity and it contributes to rise the Reynolds number for the mixture, a case with a reduced gas velocity is proved. Figure 33 shows the velocity vector plots for different planes below inlet for superficial inlet velocities of 0.066 m/s for air and water.

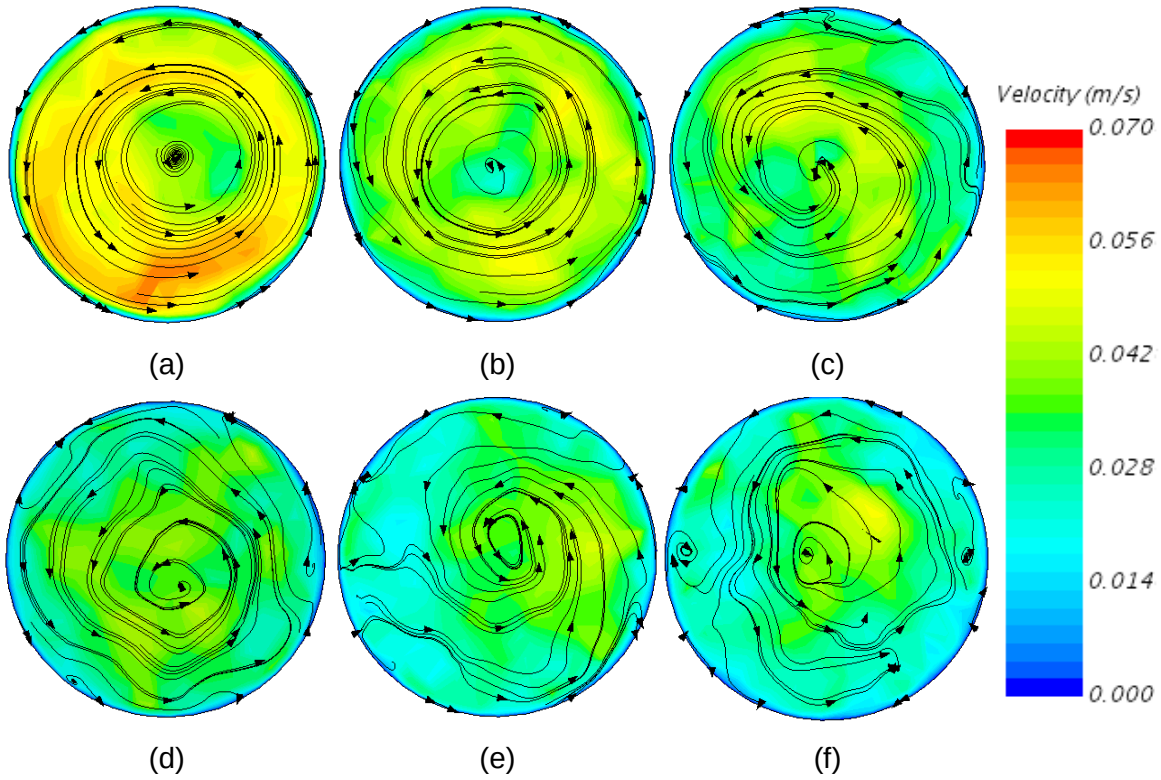

Figure 33. Swirling flow in the GLCC visualized in velocity vector plots at planes below the inlet located at (a) -5 cm (b) -10 cm (c) -15 cm (d) -20 cm (e) -25 cm and (f) -30 cm, for inlet velocities of $V_{sG} = 0.066\ m/s$ *and* $V_{sL} = 0.066\ m/s$

From Figure 33 it can be observed that the swirling flow is evidenced in lower regions than in the previous case. Taking this into account and that the Reynolds number of mixture in this case is of 2,068 it is clear that this dimensionless number is not a good indicator of the swirling flow and that the superficial velocity of liquid seems to has a more significant effect than the superficial velocity of gas. In this order of ideas, if only the Reynolds number of liquid is analyzed, it presents a value of 1,034 in the first case, 517 in the second case and 1,034 in the third case. The lowest value is obtained in the second case, the one that presents the faster swirl decaying. A fourth case is proved reducing superficial velocities from the second case. Figure 34 shows velocity vector plots in different planes below inlet for superficial velocities of 0.16 m/s and 0.016 m/s for air and water, respectively.

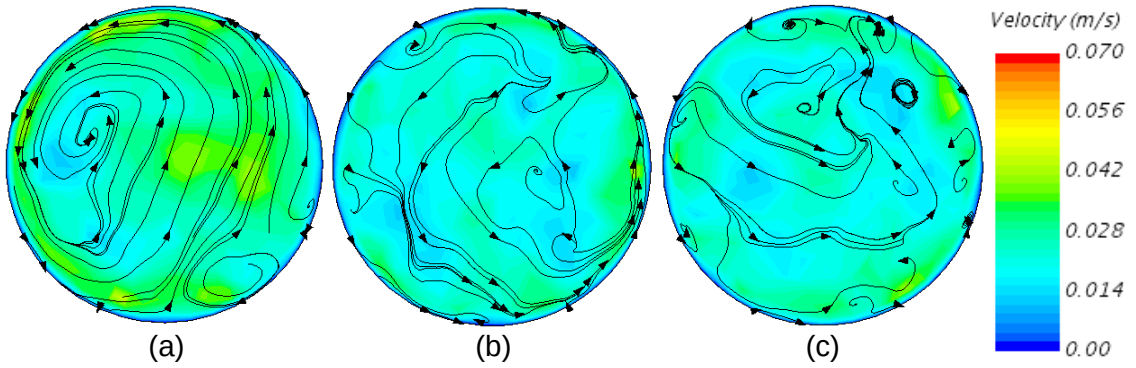

Figure 34. Swirling flow in the GLCC visualized in velocity vector plots at planes below the inlet located at (a) -5 cm (b) -10 cm (c) -15 cm, for inlet velocities of $V_{sG} = 0.16\ m/s$ *and* $V_{sL} = 0.016\ m/s$

From Figure 34 it is evidenced that the swirl is very weak, even in the plane located 5 cm below the inlet the swirl is not as clear as in the previous cases. The Reynolds number for mixture and for liquid are 2,842 and 258, respectively. In this case, the velocity at the inlets are very low and no swirl is generating major centrifugal forces in the GLCC.

6. Conclusions and recommendations

- From the results obtained in this work, it is clear that CFD simulations are capable to reproduce experimental data and to predict the behavior of the separation process inside a GLCC. The single-phase simulations shows that the swirling flow is well represented. The two-phase flow cases shows that the zero-net liquid flow with a stagnant inlet has great agreement with experimental data and shows the importance and the effect of the boundary conditions.
- For the different geometrical variables analyzed, it is clear that the GLCC configuration plays an important role in order to mitigate LCO. An angle of 27° for the inclination of the tangential inlet, an inlet 10 cm above the center of the GLCC, a dual inlet with 20 cm of distance between both inlets and a nozzle with an area of 25% of the pipe inlet are the cases where a reduction in the amount of LCO is evidenced. In the case of the volute inlet with rectangular slot, a light improvement is observed for an area of the rectangular slot of 15% of the pipe inlet. When the combination of the best cases in each variable is done, a reduction in 98% of initial LCO is obtained.
- These modifications may not be suitable for all operational cases, and should be proved with other operating conditions. Additionally, other values of the evaluated geometrical variables could be tested to improve the results and variation in other parameters that remain constant should be evaluated. These parameters are the length of the inclined section of the tangential inlet, the length of the nozzle and the length of the upper inlet in the dual inlet case.
- In the case of the study of the swirling flow decaying, it was found that at very low Reynolds number (<300) of liquid in the inlet of the GLCC a very weak swirl is evidenced. In addition, the velocity of the liquid phase seem to have a bigger effect on the swirling decaying than the velocity of gaseous phase.

Acknowledgement

The author is grateful with Dr. Nicolás Ratkovich for the support and the advices given during the development of this research project. Special thanks to Miguel Daza for his constant collaboration. The author is also grateful with the University of Tulsa and Dr. Sunday Kanshio for sharing experimental data to validate the CFD simulations.

Nomenclature

Q_L:	Flowrate of liquid	[LPM]
V_{sL}:	Superficial liquid velocity	[m/s]
Q_G:	Flowrate of gas	[LPM]
V_{sG}:	Superficial gas velocity	[m/s]
u:	Velocity in x-axis	[m/s]
v:	Velocity in y-axis	[m/s]
w:	Velocity in z-axis	[m/s]
S_M:	Momentum source term	[N*m]
HL:	Average Liquid Holdup	[-]
Re_M:	Reynolds number for mixture	[-]
D:	Diameter	[m]

Greek Letters

ρ:	Density	[m^3/s]
μ:	Dynamic viscosity	[Pa/s]
κ:	Turbulent kinetic energy	[J/kg]
ε:	Turbulent dissipation rate	[J/kg*s]
α:	Volume fraction	[-]

Abbreviations

GLCC:	Gas-Liquid Cylindrical Cyclone
LCO:	Liquid Carry Over
GCU:	Gas Carry Under
CFD:	Computational Fluid Dynamics
CAD:	Computer-Aided Design
RANS:	Reynolds-Averaged Navier-Stokes
LDV:	Laser Doppler Velocimeter
ERT:	Electrical Resistance Tomography
WMS:	Wire Mesh Sensor
CFL:	Courant-Friedrich-Levy
VOF:	Volume of Fluid
RMS:	Root Mean Square

References

Abdelsalam, A., Cem, S., & Pereyra, E. (2016). New dimensionless number for gas-liquid flow in pipes. *International Journal of Multiphase Flow*.

Adebare, A. (2006). *Optimizing the efficiency of cylindrical cyclone gas/liquid separators for field applications.* Msc Thesis, Texas A&M University.

Arpandi, I. A. (1995). *A mechanistic model for two-phase flow in gas-liquid cylindrical cyclone separators.* University of Tulsa, the Graduate School.

Avila, C., Wang, S., Gomez, L., Mohan, R., & Shoham, O. (2003). *Mathematical Modeling for integrated three-phase compact separators.* The Instrumentation, Systems and Automation Society.

Brito , A., & Trujillo, J. (2009). *Viscosity Effect in Cyclone Separators.* Society of Petroleum Engineers.

CADETEP, Universidad Simón Bolívar. (n.d.). *Separadores de vórtice.* Caracas, Venezuela.

CD-Adapco. (2016). *STAR-CCM+ User Guide.*

Celik, B., Ghia, U., Roache, J., Freitas, J., Coleman, H., & Raad, P. (2008). *Procedure for estimation and reporting uncertainity due to discretization in CFD applications.* Journal of Fluids Engineering.

Chirinos, W., Gomez, L., Wang, S., Mohan, R., Shoham, O., & Kouba , G. (2000). *Liquid Carry-Over in Gas/Liquid Cylindrical Cyclone Compact Separators.* SPE Journal.

Deparment of Ocean Engineering, MIT. (2011). *Marine Hydrodynamics.*

Erdal, F. M. (2001). *Local Measurements and Computational Fluid Dynamics Simulations in a Gas-Liquid Cylindrical Cyclone Separator.* PhD Thesis, University of Tulsa.

Erdal, F. M., Shirazi, S. A., Shoham, O., & Kouba, G. E. (1997). *CFD Simulation of Single-Phase and Two-Phase Flow in Gas-Liquid Cylindrical Cyclone Separators.*

Erdal, F., Mantilla, I., Shirazi, S., & Shoham, O. (1998). *Simulation of free interface shape and complex two-pahse flow behavior in a Gas-Liquid Cylindrical Separator.* ASME Fluids Engineering Division Summer Meeting.

Erdal, F., Shirazi, S., Mantilla , I., & Shoham, O. (2000). *Computational Fluid Dynamics (CFD) Study of Bubble Carry-Under in Gas-Liquid Cylindrical Cyclone Separators.* SPE Production & Facilities.

Frising, T., Noik, C., & Dalmazzone, C. (2005). *The Liquid/Liquid Sedimentation Process: From Droplet Coalescence Technologically Enhanced Water/Oil Emulsion Gravity Separators: A Review.* Journal of Dispersion Science and Technology.

Gomez, L. (2001). *Dispersed two-phase swirling flow characterization for predicting gas carry-under in Gas-Liquid Cylindrical Cyclone compact separators.* PhD Thesis, University of Tulsa.

Grupta, A., & Kumar, R. (2006). *Three dimensional turbulent swirling flow in a cylinder.* International Journal of Heat and Fluid Flow.

Guzmán, N. M. (2005). *Foam flow in Gas-Liquid Cylindrical Cyclone (GLCC) compact separator.* Phd Thesis, University of Tulsa.

Hreiz, R., Gentric, C., & Midoux, N. (2011). *Numerical investigation of swirling flow in cylindrical cyclones.* Chemical Engineering Resarch and Design, Elsevier.

Hreiz, R., Gentric, C., Midoux, N., & Lainé, R. (2014). *Hydrodynamics and velocity measurements in gas-liquid swirling flows in cylindrical cyclones.* Chemical Engineering Research and Design, Elsevier.

Hreiz, R., Lainé, R., Wu, J., Lemaitre, C., Gentric, C., & Funfschilling, D. (2013). *On the effect of the nozzle design on the performances of gas-liquid cylindrical cyclone separators.* International Journal of Multiphase Flow, Elsevier.

Kanshio, S. (2015). *Multiphase Flow in Pipe Cyclonic Separator.* PhD Thesis. Cranfield University. Oil and Gas Engineering Centre.

Kanshio, S., Yeung, H., & Lao, L. (2015). *The experimental study of liquid holdup in gas-liquid pipe cyclonic separator using electrical resistance tomography and wire mesh sensor.* Cranfield University, UK: Oil and Gas Engineering Centre. BHR Group.

Kouba, G. E., & Shoham, O. (1996). A review of Gas-Liquid Cylindrical Cyclone (GLCC) Technology. *Production Separation Systems International Conference.* Aberdeen, UK.

Mantilla, I. (1998). *Bubble trajectory analysis in Gas-Liquid Cylindrical Cyclone Separators.* MSc Thesis, University of Tulsa.

Marti, K., Erdal,, F., Shoham, O., Shirazi, S., & Kouba, G. (1996). *Analysis of gas carry.under in Gas-Liquid Cylindrical Cyclones.*

Movafaghian, S. (1997). *The effects of geometry, fluid propereties and pressure on the flow hydrodynamics in Gas-Liquid Cylindrical Cyclone Separators.* Msc Thesis, University of Tulsa.

Movafaghian, S., Jaua-Marturet, J. A., Mohan, R. S., Shoham, O., & Kouba, G. E. (2000). *The effects of geometry, fluid properties and pressure on the hydrodynamics of gas-liquid cylindrical cyclone separators.* International Journal of Multiphase Flow, Pergamon.

Najafi, A., Saidi, M., Sadeghipour, M., & Souhar, M. (2005). *Numerical analysis of turbulent swirling decay pipe flow.* International Communications of Heat and Mass Transfer.

Shoham, O., & Kouba, G. E. (1998). *State of the Art of Gas/Liquid Cylindrical-Cyclone Compact Separator Technology.* SPE Distinguished Author Series.

Steenbergen, W., & Voskamp, J. (1998). *The rate of decay of swirl in turbulent pipe flow.* Flow Measurement and Instrumentation.

Van Sy, L. (2016). Influence of inlet angle on flow pattern and performance of gas-liquid cylindrical cyclone separator. *Particulate Science and Technology*.

Versteeg , H., & Malalasekera, W. (2007). Introduction. In *An Intoduction to Computational Fluid Dynamics* (pp. 1-6). Pearson Education.

Appendix A – Photos of the experimental setup performed at Universidad de los Andes

Figure A 1. General view of the experimental setup performed

Figure A 2. Pressure transmitter and power supply

Figure A 3. GLCC frontal view

Appendix B – Tabulated results of the evaluated geometrical modifications

Table B 1. CFD results of LCO and GCU for the five geometrical variables

Geometry variable	Case	LCO (mL/s)	GCU (kg/s)
Inclination angle of the tangential inlet	0	7.23	2.18E-08
	13	6.54	3.44E-08
	27	5.74	3.02E-08
	41	5.66	2.39E-08
	55	7.54	2.10E-08
Height of the tangential inlet	Center	7.23	2.18E-08
	10 cm above center	1.83	1.97E-08
	10 cm below center	16.27	2.90E-08
	5 cm above center	5.39	2.03E-08
Dual inlet	Single Inlet	7.23	2.18E-08
	Dual inlet with 5 cm between both inlets	12.14	1.35E-08
	Dual inlet with 7.5 cm between both inlets	11.18	1.66E-08
	Dual inlet with 20 cm between both inlets	1.23	1.30E-08
Nozzle	Without nozzle	7.23	2.18E-08
	Nozzle of 7 mm of diameter	9.04	4.22E-08
	Nozzle of 3.5 mm of diameter	3.13	1.35E-07
	Nozzle of 1.75 mm of diameter	3.71	8.76E-08
Volute inlet with rectangular slot	Without volute inlet	7.23	2.18E-08
	Volute inlet of 25% of pipe area (9.62 mm of height and 4 mm of width)	6.75	4.31E-08
	Volute inlet of 25% of pipe area (19.24 mm of height and 2 mm of width)	6.91	3.43E-08
	Volute inlet of 25% of pipe area (4 mm of height and 9.62 mm of width	7.25	4.90E-08
	Volute inlet of 15% of pipe area (6.597 mm of height and 3.5 mm of width)	5.61	4.39E-08

Appendix C – CFD complementary images

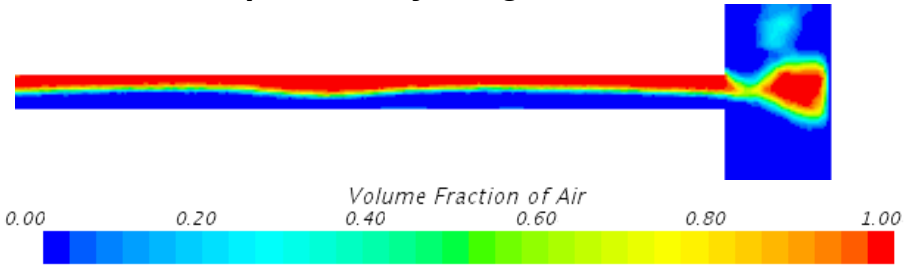

Figure C 1. Flow pattern in the inlet pipe of the GLCC